Article

Developmental Cell

Host-transposon mutualism supports regeneration in planarians

Graphical abstract

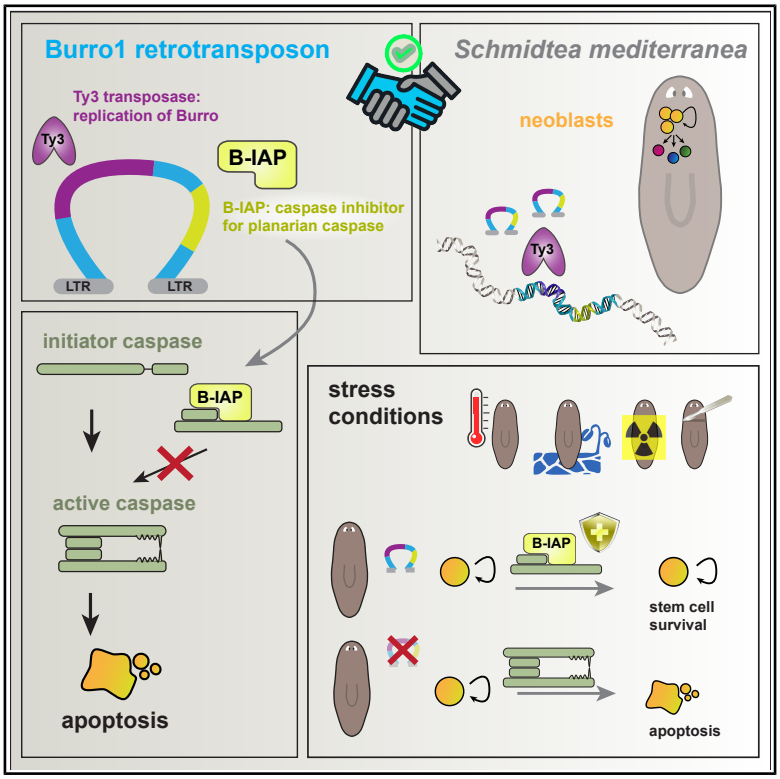

Highlights

- Burro1 is a composite transposon that escaped inactivation for 100 million years
- Burro1 captured an anti-apoptotic host gene (*B-iap*) that yields a functional protein
- Burro1 (including *B-iap*) transcription is upregulated during stress
- Stress-induced B-IAP enhances stem cell survival and planarian regeneration

Authors

Hae-Lim Lee, Axel Poulet, Sudheesh Allikka Parambil, Josien C. van Wolfswinkel

Correspondence

josien.van.wolfswinkel@yale.edu

In brief

Lee et al. find that the planarian transposon Burro1 bolsters stem cell resilience by producing a functional host-derived caspase inhibitor during physiological stress. By suppressing apoptosis, active Burro1 elements enhance the regenerative capacity of planarians and have sustained this mutualistic relationship for over 100 million years.

Lee et al., 2026, Developmental Cell *61*, 1–15
May 13, 2026
https://doi.org/10.1016/j.devcel.2026.03.001

CellPress

Please cite this article in press as: Lee et al., Host-transposon mutualism supports regeneration in planarians, Developmental Cell (2026), https://doi.org/10.1016/j.devcel.2026.03.001

Developmental Cell

CellPress
OPEN ACCESS

Article

Host-transposon mutualism supports regeneration in planarians

Hae-Lim Lee,[1] Axel Poulet,[1] Sudheesh Allikka Parambil,[1] and Josien C. van Wolfswinkel[1,2,3,4,5,*]
[1]Department of Molecular Cellular and Developmental Biology, Yale University, New Haven, CT 06511, USA
[2]Yale Stem Cell Center, Yale School of Medicine, New Haven, CT 06511, USA
[3]Yale Center for RNA Science and Medicine, Yale School of Medicine, New Haven, CT 06511, USA
[4]Yale Center for Research on Aging (Y-Age), Yale School of Medicine, New Haven, CT 06511, USA
[5]Lead contact
*Correspondence: josien.van.wolfswinkel@yale.edu
https://doi.org/10.1016/j.devcel.2026.03.001

SUMMARY

Transposons make up a significant fraction of eukaryotic genomes. They are commonly viewed as selfish elements that are detrimental to their hosts, and they are prime targets of specialized host defenses that constrain their expansion. Mutualistic interactions, in which elements co-exist and benefit each other, have so far not been found between transposable elements and eukaryote hosts.

Here, we present evidence for an active transposon that confers a direct benefit to its planarian host. We find that the Ty3-like giant transposon Burro1 is an ancient element that retains its mobility. Burro1 has incorporated a host-derived anti-apoptotic protein that upregulates upon stress and improves stem cell resilience, resulting in enhanced regenerative abilities in its host.

Apart from the surprising finding of a transposon's involvement in planarian regeneration, our data also uncover a true mutualistic interaction between a transposon and a eukaryote host.

INTRODUCTION

Transposons are widely present in the genomes of eukaryotes and can occupy as much as 85% of the host genome.[1,2] They are commonly viewed as selfish elements that expand and evolve without any particular benefit to their host.[3,4] In fact, they add genomic ballast, their repetitive nature can facilitate undesired recombination events, and their capacity to jump to new genomic locations can disrupt existing elements, supporting their reputation as a threat to their host's genomic integrity.[5] Eukaryotes employ a range of mechanisms to defend against transposon activity, and the interaction between transposons and their hosts has been described as an arms race, in which the host fights to inactivate the transposon while the transposon develops an escape mechanism or dies.[6]

This adversarial relationship between transposons and eukaryotes forms a stark contrast with the situation in prokaryotes, where mutually beneficial arrangements between mobile genetic elements and their hosts are commonplace. To compensate for their negative effects, prokaryotic plasmids frequently carry genes that improve the host's resistance against heavy metals and antibiotics or improve the acquisition of nutrients.[7–10] Prokaryote composite transposons are known to carry similar genic contributions,[11,12] thereby forming a reciprocal relationship with their host in which each provides a direct fitness benefit to the other that outweighs the burden of the partnership. Such an enduring and reciprocal mutualistic interaction favors not only the survival and propagation of the host but also the persistence of the functional transposon.

Eukaryotic hosts have adapted to the presence of transposons in their genomes and, in some cases, make good use of transposon-derived sequences,[13] but surprisingly no true reciprocal mutualisms have been found. The chromatin organization of many eukaryotes, for example, uses the abundance of transposons around telomeres and centromeres to form heterochromatic regions and uses transposon-contributed CTCF (CCCTC binding factor) binding sites.[14–20] Additionally, transposons represent a significant source of novel genetic material. Their sequences may introduce new enhancer elements that modify the expression of neighboring genes,[21–24] and transposon-derived (fusion) proteins have taken on essential functions or have enabled evolutionary novelties, including the Telomerase Reverse Transcriptase (TERT), the Centromere Protein B (CENP-B), the histone methyltransferase Setmar, the Recombination Activating Genes (RAG) that mediate VDJ (variable-diversity-joining) recombination in the vertebrate immune system, and the cell-cell fusion protein Syncytin that is essential for placental development.[25–36] Although derived from transposons, these sequences have been domesticated: they no longer mobilize and the remaining (incomplete) sequences are under host control. Such beneficial effects thus may shift the balance toward tolerance of transposons in eukaryote genomes over evolutionary time scales; however, they do not contribute to the retention of active transposable elements. Recently, some cases of

Please cite this article in press as: Lee et al., Host-transposon mutualism supports regeneration in planarians, Developmental Cell (2026), https://doi.org/10.1016/j.devcel.2026.03.001

active transposons intertwined with the host physiology have been reported, but these are thought to reflect addictions: instances in which a host process was initially disrupted by the transposon, and the host adaptation to bypass this disruption can function only in the presence of the transposon.[6,37–40] Although this makes the transposon indispensable, it provides no net benefit to the host. Furthermore, in each of these cases, the repurposed sequences are core transposon genes required for their replication and thus constitute no fitness cost to the transposon, thereby upholding their reputation as purely selfish elements.

Genome sequencing of the planarian *Schmidtea mediterranea* recently uncovered a remarkable transposon family called Burro (big unknown repeat rivaling ogre) that consists of three long terminal repeat (LTR) transposons of giant proportions.[41] Burro transposons belong to the Ty3 superfamily (also known as Gypsy or *Metaviridae*). Burro elements are between 30- and 35-kb long and contain several additional open reading frames (ORFs) besides the Ty3 polyprotein, which comprises the essential proteins for mobilization.[42,43] These additional ORFs are unrelated to the core transposon genes, suggesting that they have no role in the replication or insertion of the transposon itself; however, their function has remained unresolved.

One of the Burro elements, Burro1, is remarkable not only because of its size but also because it has achieved a high copy number and occupies a significant fraction of the *S. mediterranea* genome.[41] Here, we set out to analyze the life history of this successful giant transposon and its additional ORFs, as well as the biological relevance of these additional sequences.

RESULTS

Burro1 is an ancient, highly prolific transposon

The 35-kb consensus sequence of Burro1 consists of one large ORF encoding the Ty3 polyprotein, which includes the protease, reverse transcriptase (RT), ribonuclease H (RNase H), and integrase, as well as a 5′ extended region (Figure 1A).[41–43] The polyprotein is flanked at the 3′ end by several smaller ORFs. The 3′ and 5′ termini of the transposon consist of 5-kb LTRs. The sequence of the core Ty3 polyprotein is similar among Burro1, Burro2, and Burro3, but the additional ORFs 3′ of the polyprotein, as well as the 5′ extended regions of the polyprotein and the LTRs, are distinct among the three family members (Figure S1A).

Ty3 retrotransposons comprise over 25% of the *Schmidtea* genome (Figure 1B). Among these, Burro1 has been particularly prolific: it covers an estimated 8% of the genomic sequence, making it the single most prominent element. Although most Burro1 copies are truncated, 289 intact copies remain based on the current assembly (Figure S1B). Because the presence of such long repetitive elements complicates genome assembly,[41] we used qPCR as an assembly-independent method to estimate the number of Burro1 copies in the *Schmidtea* genome. Using multiple independent primer sets, we found that the total number of Burro1 copies was consistent with the number in the assembled genome (Figure 1C), indicating that the assembled genome provides an accurate representation of the Burro1 landscape.

We used two methods to estimate the age of Burro1: sequence divergence and phylogeny. Assuming a stable rate of base substitutions, quantification of the sequence divergence between the current copies and the consensus sequence gives a relative estimate of a transposon's age compared with other transposons.[44] Divergence analysis revealed that a significant subset of Burro1 elements exhibited higher divergence from the consensus compared with other Ty3 elements, suggesting that it is one of the oldest Ty3 families in the planarian genome (Figure 1D).[41] We also investigated when in flatworm evolutionary history Burro1 was first introduced. We confirmed its previously reported presence in *Girardia tigrina*,[42] and also found evidence of its expression in *Schmidtea polychroa*, *Dugesia japonica*, and *Girardia dorotocephala* (all members of the *Dugesiidae*), as well as in *Bipalium kewense* (*Geoplanidae*). We, however, failed to detect Burro1 in *Macrostomum lignano* (*Macrostomidae*; outgroup) or in any of the members of the *Planariidae* or *Dendrocoelidae* (Figure 1E). This suggests that Burro1 first arose within the *Geoplanoidea* after they had split off from the *Dendrocoelidae* and the *Planariidae* (Figure 1E). The split between *Dugesiidae* and *Geoplanidae* is estimated to have occurred over 135 million years ago (mya),[45,46] thereby dating Burro1 as over 100 million years old.

Transposons typically go through life cycles[47]: initially, a new transposon rapidly expands to become established in the genome, resulting in the presence of many copies with high mutual similarity. Later, activity is reduced, often leading to the death of the transposon,[48,49] which is reflected by transposons with fewer copies and high inter-copy divergence. To determine where Burro1 falls on this spectrum, we compared divergence and copy numbers of Ty3 transposons in the *Schmidtea* genome. Most elements followed the pattern described, showing either high copy numbers with low divergence or low copy numbers with high divergence (Figure 1F). Burro1, however, exhibited both high mean divergence and high copy number. This suggests that the regulation of Burro1 is atypical and that Burro1 has retained its activity.

To evaluate the recent activity of the Burro transposons, we compared the 5′ and 3′ LTRs of full-length retrotransposon copies (Figure 1G). Because the two LTRs must have been identical at the time of insertion and have diverged over time,[50] copies with identical LTRs serve as markers of recent activity. Indeed, the ancient transposon Gypsy14 showed no copies with identical LTRs, whereas the currently active transposon SLF9 had many. For Burro1, while many elements had diverging LTRs, suggesting older insertions, 13% of the elements had LTRs with over 99% identity, providing strong evidence of recent activity (Figure 1G). Further, we serendipitously found at least one fully intact insertion of Burro1 that is present in the sexual strain of *S. mediterranea* and absent from the asexual strain (Figure S1C). These strains are thought to have diverged around 1 mya, indicating that Burro1 has been recently active.

Together, these data indicate that Burro1 is an ancient transposon that entered the flatworm genome over 100 mya, after the split of *Geoplanoidea* from other planarian branches. Burro1 effectively expanded and, surprisingly, shows signs of continued conservation and activity in the *S. mediterranea* genome.

Burro is composed of elements pre-existing in the planarian genome

To determine the origin of Burro1, we analyzed the phylogenetic relationships of its various parts with related elements in metazoan

Please cite this article in press as: Lee et al., Host-transposon mutualism supports regeneration in planarians, Developmental Cell (2026), https://doi.org/10.1016/j.devcel.2026.03.001

CellPress
OPEN ACCESS

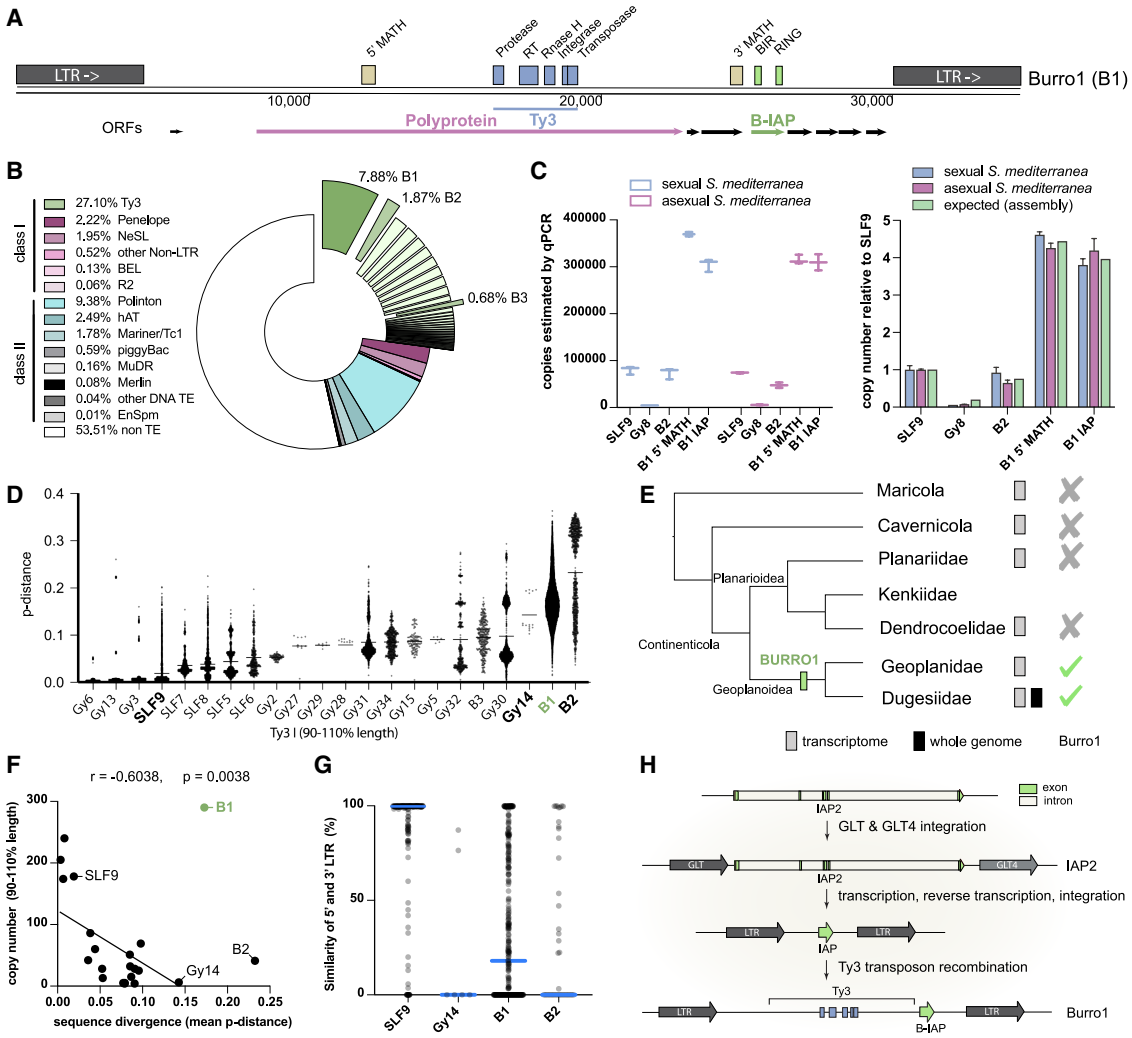

Figure 1. Life history of Burro1

(A) Schematic of ORFs (arrows) and conserved protein domains (boxes) in Burro1. Burro1 contains several downstream ORFs, some of which contain conserved protein domains.

(B) The *Schmidtea mediterranea* genome contains both RNA transposons (class I) and DNA transposons (class II). Burro1 (B1) is the most prominent element in the genome. Also highlighted are Burro2 (B2) and Burro3 (B3).

(C) qPCR quantification of several Ty3 elements in the *S. mediterranea* genome. The estimated copy number of B1 (left) is in line with the expectation based on the genome assembly (right). Data are shown as mean ± SD; $n = 3$ independent samples of 20 animals each.

(D) Sequence divergence (Kimura distance) is shown as a measure of age of the most abundant Ty3 elements. A line indicates the mean. B1 has copies with a wide range of divergences, indicating that it is one of the oldest transposons in the genome and has remained active over a long period. The transposons highlighted in (F) and (G) are marked in bold. Only full-length elements (90%–110% of consensus length) were included in the analysis. Horizontal lines represent mean values.

(E) Phylogenetic tree of platyhelminths showing the presence and absence of Burro1, indicating that Burro likely originated within the *Geoplanoidea*.

(F) Scatterplot with linear regression showing the correlation between retained copy number and sequence divergence (age) among Ty3 elements. B1 is an outlier that has retained a higher number of copies than expected based on its estimated age.

(G) Similarity of 5′ and 3′ LTRs among retained copies of Ty3 elements. The median values are indicated in blue. The existence of B1 copies with identical LTRs suggests recent integrations.

(H) Schematic of the hypothesized origination of the B1 element (see supplemental information for further details).

See also Figures S1 and S2.

and viral genomes. The RT and integrase sequences of the three Burro elements were closely related to each other and resembled those of other Ty3-related elements in the *Schmidtea* genome (Figure S1D). This suggests that the core Ty3 component of Burro likely originated from within the planarian genome rather than from horizontal gene transfer. The LTRs of the three Burro elements were not related, and each resembled LTRs from different planarian Ty3 elements (Figure S2A), indicating that the three Burro transposons likely originate from a single active Ty3 core element that acquired different LTRs (Figure S2C).

Please cite this article in press as: Lee et al., Host-transposon mutualism supports regeneration in planarians, Developmental Cell (2026), https://doi.org/10.1016/j.devcel.2026.03.001

The most distinctive features of the Burro elements are the ORFs downstream of the polyprotein, which also differ among the three Burro transposons. Several of the ORFs were small and showed no similarity to any known protein or nucleic acid sequences, but two ORFs in Burro1 contained recognizable protein domains, suggesting that they may have conserved functionality (Figure 1A). The first ORF downstream of the polyprotein contained a MATH (Meprin and TRAF-C homology) domain and showed similarity to tumor necrosis factor (TNF)-receptor associated proteins (TRAFs). The Burro-encoded ORF was similar between Burro1 and Burro2 and was closely related to other planarian MATH domain proteins (Figures S1A and S2B). This protein family is highly expanded in the planarian genome, encompassing well over 100 sequences.[51] Their function has not been resolved, as the planarian genome does not encode a clear homolog of TNF or of the TNF receptor, and many of the TRAF-related genes lack the domain organization typical of TRAF proteins in other systems.

The second long downstream ORF of Burro1 encoded a protein with a well-conserved BIR(Baculovirus IAP repeat) domain and a RING (really interesting new gene) domain, which are characteristic of the Baculoviral inhibitor of apoptosis (IAP) family.[52,53] Members of this protein family are found in eukaryotes, prokaryotes, and viruses and are categorized into two different types. Proteins with type I BIR domains (which include vertebrate c-IAP (cellular IAP), XIAP (X-linked IAP), and NAIP (neuronal apoptosis inhibitory protein) typically exhibit caspase-binding activity and function in the regulation of programmed cell death, whereas type II BIR domains are found in eukaryote proteins involved in the regulation of cell cycle (such as vertebrate proteins Bruce and Survivin). Viral BIR domains are diverse, suggesting that they do not have a monophyletic origin (Figure 2A).

To determine the origin of the Burro1 BIR-domain protein, we performed a phylogenetic analysis. We identified 5 other BIR-domain proteins in the *Schmidtea* genome, of which the two type I BIR domains (from IAP-1 and IAP-2; Figures 2A and S1E) clustered closely with the Burro1 BIR domain. We therefore refer to the Burro1-encoded protein as Burro-IAP (B-IAP). Interestingly, *iap-1* and *iap-2* had very similar exon structures and retained considerable sequence similarity. *B-iap*, which lacks introns, had 47.8% identity to *iap-2*, suggesting that it originated from a cDNA copy of this gene.

Taken together, these analyses suggest that Burro1 was formed by combining several elements that pre-existed in the planarian genome (Figures 1H and S2C). The downstream ORFs are closely related to their genomic genic counterparts, indicating that they are likely of planarian origin rather than acquired by horizontal gene transfer.

B-IAP is a conserved protein and is expressed in planarian neoblasts

To identify the functional elements in Burro1, we analyzed its DNA sequence across planarian species to evaluate signs of evolutionary pressure. As expected, the core Ty3 protein region showed clear sequence conservation among the different species (Figure 2B). Interestingly, we detected a second region of conservation covering the downstream ORF that corresponds to B-IAP. Because some changes in DNA sequence result in conservation of the amino acid sequence, we analyzed the ratio of synonymous to non-synonymous changes in the various elements of Burro1 (Figure 2B). Although non-synonymous mutations were common in the 5′ extended region of the polyprotein and in the 3′ additional ORFs, the core Ty3 region and the *B-iap* region showed notably lower levels of amino acid substitutions. This indicates that the B-IAP protein is under selective pressure, suggesting that it is functionally important.

Active protein translation typically takes place on polysomes, whereas non-coding or aberrant transcripts are retained on monosomes and degraded. To determine whether *B-iap* was translated into protein, we used qPCR to analyze the distribution of the *B-iap* transcript between monosomes and polysomes (Figure 2C).[55] Similar to coding genes, the *B-iap* transcript was enriched on polysomes, suggesting that it is actively translated. To identify the protein product, we raised and affinity purified a B-IAP-specific antibody (Figure S3A). Application of this antibody to planarian lysates revealed a specific band around 50 kDa that was reduced upon the RNAi-mediated knockdown of Burro1 (Figure 2D), indicating that the Burro1-encoded *B-iap* sequence indeed produces a full-length protein product in planarian cells.

We inspected RNA sequencing (RNA-seq) data from various isolated tissues[54] to determine the expression pattern of *B-iap* and to compare it with the two genomic *iap* genes. We found that *iap-1* and *iap-2* were broadly expressed at low levels, whereas *B-iap* was more highly expressed. *iap-2* was enriched in epidermis and intestine, whereas *iap-1* and *B-iap* were clearly detected in the adult pluripotent stem cells of planarians, known as neoblasts (Figure 2E). This observation was confirmed by public single-cell sequencing data[56] (Figure S3B) and by qPCR analysis on isolated neoblasts (Figure S3C). We next used fluorescent *in situ* hybridization (FISH) to independently verify the tissue distribution of *B-iap* (Figure 2F). In agreement with the RNA-seq data, *iap-2* was mostly present in subsets of epidermal and intestinal cells. The *B-iap* transcript was detected at higher intensity and was enriched in parenchymal cells, which include the neoblasts. FISH on dissociated cells as well as on whole mounts confirmed that *B-iap* expression was detected in the same cells as the neoblast-specific marker *smedwi-1* (Figures 2G and S3D). Using the B-IAP antibody, we found that some of the B-IAP protein was localized to foci associated with stem cells (Figures 2H and S3E). To specifically investigate the intracellular protein, we analyzed B-IAP in dissociated cells co-stained with markers for specific cell types. This analysis showed that B-IAP protein was present in neoblasts (Figures 2I and S3F) and in intestinal cells (Figure S3G), but not in epidermal cells.

B-IAP is upregulated in response to stress

While exploring the expression of the planarian *iap* genes, we found that *B-iap* levels significantly increased immediately upon amputation, whereas the other *iap* transcripts were not affected (Figures 3A, S3H, and S3I). This effect was confirmed by reanalysis of previously published sequencing data from a regeneration time course[57] (Figure S3J). The *B-iap* transcript was detected throughout the tissue fragment and notably included expression in the neoblasts (Figure 3B). Although levels of the Piwi transcript *smedwi-1* were slightly decreased after amputation, suggesting a possible loss of transposon silencing, SMEDWI-1 protein levels remained unaffected. Furthermore, knockdown of *smedwi-1* failed to increase *Burro1* or *B-iap* levels (Figures S3K–S3M). These

Please cite this article in press as: Lee et al., Host-transposon mutualism supports regeneration in planarians, Developmental Cell (2026), https://doi.org/10.1016/j.devcel.2026.03.001

CellPress
OPEN ACCESS

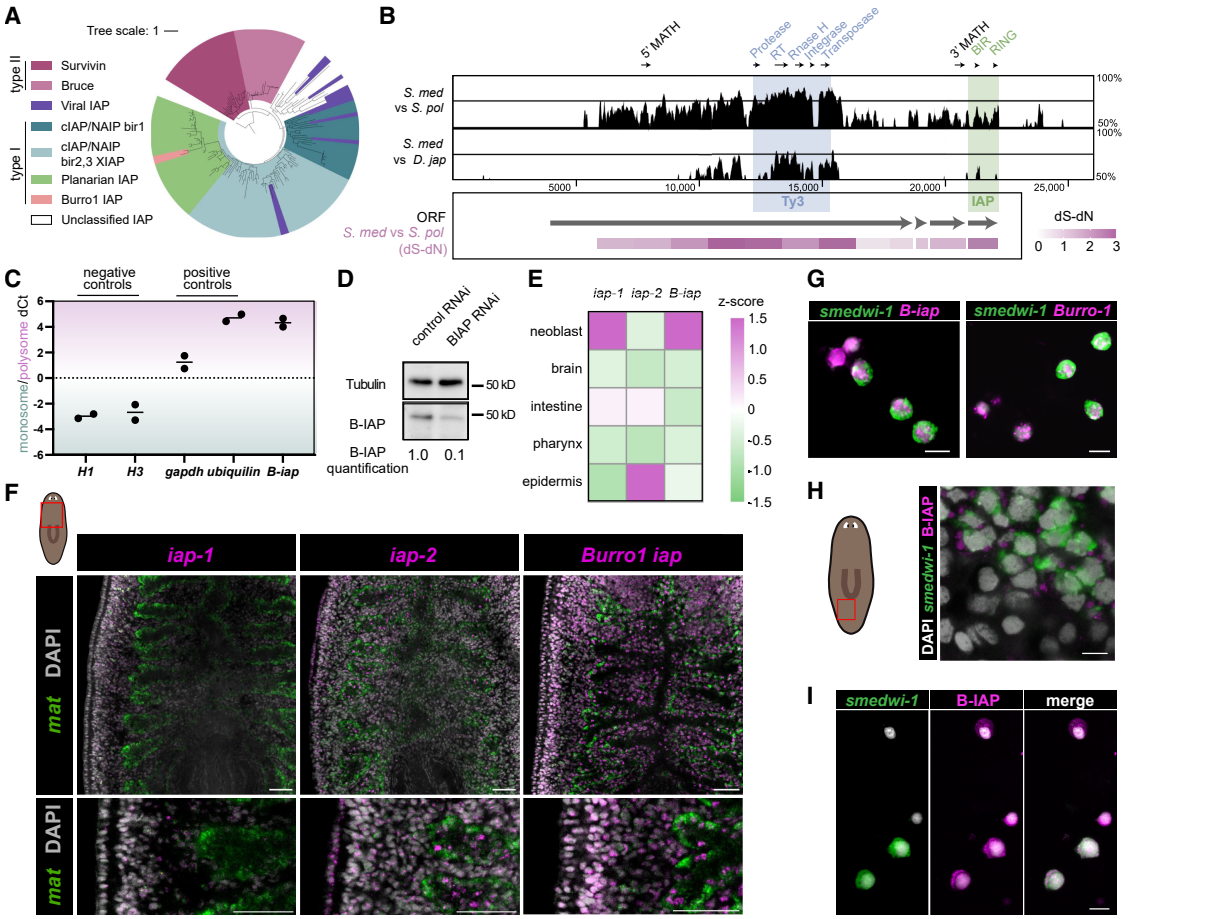

Figure 2. *B-iap* is expressed in planarian neoblasts

(A) Phylogenetic tree of metazoan BIR domains showing that Burro-IAP (B-IAP) is most closely related to other planarian type I BIR-domain proteins.

(B) Top: graph of the percentage of sequence similarity between Burro1 sequences from various *Dugeasiidae* species, showing sequence conservation in the core Ty3 domain as well as in the B-IAP region. Bottom: heatmap representing the rate of synonymous vs. non-synonymous mutations (dS-dN) in the different coding regions of Burro1.

(C) qPCR quantification of RNA associated with monosomes (untranslated, green) and polysomes (actively translated transcripts, magenta) shows enrichment of *B-iap* transcripts on polysomes, suggesting active translation. Housekeeping genes are shown as positive controls, whereas histone transcripts that are not actively translated outside S phase are used as negative controls. Values from two independent polysome fractionations are shown.

(D) Western blot showing the presence of the B-IAP protein in planarian lysate.

(E) Heatmap representing *Z* scores of expression levels from isolated planarian tissues.[54] *B-iap* is enriched in the neoblasts compared with other tissues.

(F) Fluorescent *in situ* hybridization (FISH) on whole-mount animals showing *B-iap* or genomic *iap* transcripts (magenta) together with the intestinal marker *mat* (green). *B-iap* is expressed in the parenchymal space. The bottom images show zoomed-in sections. Scale bars, 100 μm.

(G) FISH on isolated cells shows co-expression of *B-iap* (magenta) and the stem cell marker *smedwi-1* (green). Scale bar, 10 μm.

(H) Immunostaining of intact planarians for the B-IAP protein (magenta) combined with FISH for the neoblast marker *smedwi-1* (green) shows granules of B-IAP protein associated with neoblasts. Scale bar, 10 μm.

(I) Immunostaining of dissociated cells for the B-IAP protein (magenta) combined with FISH for the neoblast marker *smedwi-1* (green) shows B-IAP protein in neoblasts. Scale bar, 10 μm.

See also Figure S3.

results indicate that the amputation-induced increase in *B-iap* is not caused by a loss of SMEDWI-1-mediated silencing.

To test whether the increase in *B-iap* was driven by increased transcription or decreased turnover, we repeated the amputations in the presence of the transcription inhibitor actinomycin D (Figure 3C). As a control, we observed that activation of the early wound-response gene *jun* was repressed by actinomycin D, confirming effective inhibition of transcription. Under these conditions, the increase in *B-iap* RNA was completely abolished. These results indicate that the amputation-induced rise in *B-iap* levels results from increased transcription. This transcriptional response preceded the activation of mitosis in the neoblasts and the increase in apoptosis detected at the wound site,[58,59] which occur at 6 and 4 h after wounding, respectively, emphasizing that *B-iap* is part of a very early response to injury. Of note, a second peak of *B-iap* expression was detected at 72 h after amputation, concomitant with an increase in the stem cell transcript *smedwi-1* (Figures S3N and S3O), indicating that

Please cite this article in press as: Lee et al., Host-transposon mutualism supports regeneration in planarians, Developmental Cell (2026), https://doi.org/10.1016/j.devcel.2026.03.001

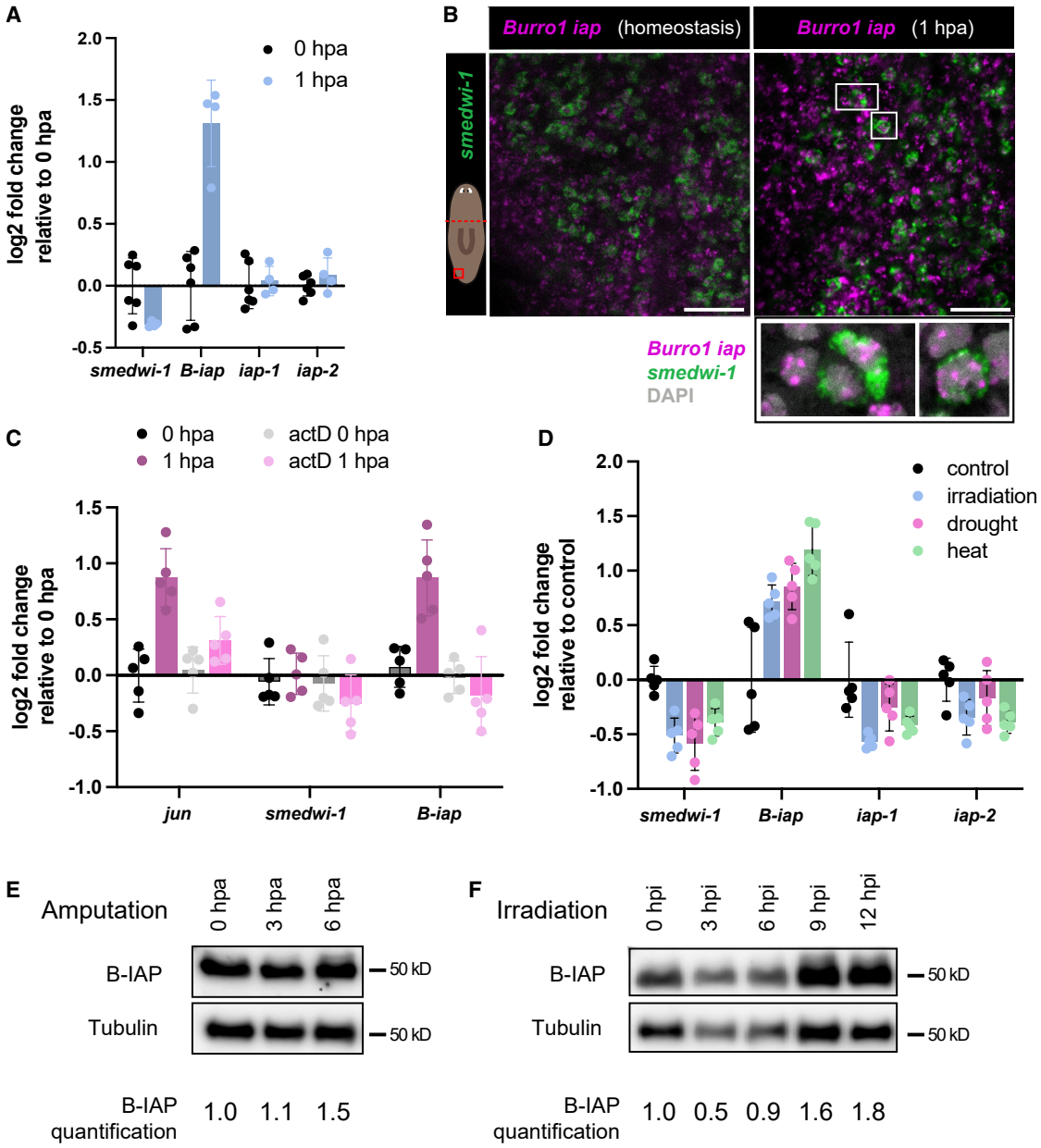

Figure 3. B-IAP is upregulated in response to stress

(A) qPCR on tissue fragments in the early hours following head amputation (hpa) shows an increase in *B-iap* transcript at 1 h after amputation. Data are shown as mean ± SD; $n = 6$ samples at 0 hpa and 4 samples at 1 hpa, each consisting of 3 animals.

(B) FISH at 1 hpa shows an increase in *B-iap* transcript (magenta) throughout the tissue fragment. Scale bars, 50 μm. Insets show expression in neoblasts by co-localization with the neoblast marker *smedwi-1* (green).

(C) qPCR at 1 hpa on tissue fragments treated with the transcription inhibitor actinomycin D or DMSO as a control shows an increase in the early wound-response transcript *jun* and in *B-iap* transcript only in the control-treated samples. Data are shown as mean ± SD; $n = 5$ independent samples of 3 animals each.

(D) qPCR at 1 h after irradiation (1,500 Rads), drought, or heat stress shows an increase in *B-iap* transcript but no change in transcripts for *smedwi-1*, *iap-1*, or *iap-2*. Data are shown as mean ± SD; $n = 5$ independent samples of 3 animals each.

(E) Western blot of planarian lysate at the indicated time points after amputation shows an increase in B-IAP protein. Quantification is relative to the tubulin signal.

(F) Western blot of planarian lysate at the indicated time points after irradiation shows an increase in B-IAP protein. Quantification is relative to the tubulin signal.

See also Figure S3.

this late increase in *B-iap* could be the result of stem cell expansion.

To test whether the transcriptional upregulation of *B-iap* extended to other forms of organismal stress, we tested *B-iap* levels upon exposure to irradiation, drought, and heat stress. We found that at 1 h after each of these stresses *B-iap* levels were strongly increased (Figures 3D and S3P), indicating that planarian cells rapidly upregulate *B-iap* transcription in response

Please cite this article in press as: Lee et al., Host-transposon mutualism supports regeneration in planarians, Developmental Cell (2026), https://doi.org/10.1016/j.devcel.2026.03.001

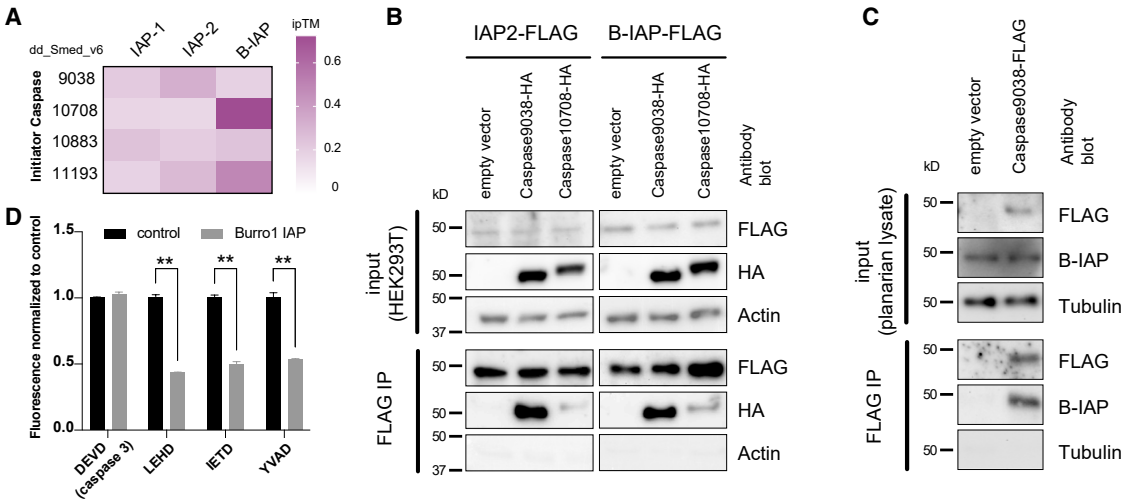

Figure 4. B-IAP is a functional anti-apoptotic protein

(A) Heatmap showing the likelihood of interaction between the three planarian IAP proteins and the various planarian caspases (dd IDs *(37)*). ipTM, confidence score for the interaction. Only the interaction between B-IAP and the initiator caspase shows significant support. For reference, the ipTM for human XIAP with caspase9 is 0.75

(B) Western blots showing coimmunoprecipitations (coIPs) of hemagglutinin (HA)-tagged caspases with FLAG-tagged IAP protein expressed in HEK293T cells. The predicted interaction between B-IAP and caspase_10708 is confirmed, but a stronger interaction with caspase_9038 is identified.

(C) Western blots showing coIPs of planarian B-IAP from planarian lysates with exogenously supplemented FLAG-tagged caspase_9038 protein.

(D) Plots showing *in vitro* caspase activity in control samples and samples supplemented with B-IAP protein. Data are shown as mean ± SD. Significance is $^{**}p \leq 0.01$ by Student's *t* test. $n = 3$ planarian lysates for each control and supplemented data point.

See also Figure S4.

to a wide range of organismal stresses. We further tested whether the detected upregulation of *B-iap* at the transcript level led to elevated B-IAP protein levels. Indeed, both amputation (Figure 3E) and irradiation (Figure 3F) resulted in notably increased levels of B-IAP protein, as detected by western blot.

B-IAP is a functional caspase inhibitor

IAP proteins are best known for their anti-apoptotic activity through direct interactions with caspase proteins.[60] The best-studied mammalian IAP protein, XIAP, contains three BIR domains. The second BIR domain binds to effector caspases (caspase-3 and -7), resulting in blocked enzymatic activity, whereas the third binds the initiator caspase, caspase-9, inhibiting its dimerization. In particular, the obstruction of caspase-9 dimerization is essential for XIAP's anti-apoptotic effect.[61] Planarians encode both effector caspases and initiator caspases (Figures S4A and S4B). We thus hypothesized that B-IAP might interact with one or more planarian caspase proteins.

To determine whether B-IAP retained the amino acid residues required for caspase inhibition, we aligned its BIR domain with well-characterized human BIR domains (Figure S4C). We found that the B-IAP lacks the residues required for enzymatic inhibition of effector caspases, but the residues for inhibition of the initiator caspases were largely retained.[62–64] Structural modeling of the B-IAP BIR domain with the planarian caspases revealed a plausible interaction with one of the four initiator caspases, whereas no such interaction was predicted for any of the effector caspases (Figures 4A, S4D, and S4E). To further explore the binding of B-IAP to initiator caspases, we cloned tagged versions of both proteins into HEK293T cells to test their interaction *in vitro* (Figures 4B, S4F, and S4G). B-IAP indeed co-precipitated with the predicted initiator caspase (caspase_10708), but we found an even stronger interaction with the related planarian initiator caspase_9038. We next used tagged caspase_9038 protein to pull down interactors from planarian lysate and indeed precipitated B-IAP protein (Figures 4C and S4H). These data demonstrate that B-IAP is a genuine caspase-binding protein.

Dimerization of human caspase-9 triggers its proteolytic activity, which activates effector caspases to cleave a large set of cellular proteins and drive the cell into apoptosis. To further evaluate the anti-apoptotic capacities of B-IAP, we expressed the protein in HEK293T cells and tested its effect on initiator caspase activity in planarian lysates (Figure S4I). We determined that the consensus cleavage site in the planarian effector caspases consists of a VLAD motif (Figure S4J), and used *in vitro* fluorometric substrates with similar peptide sequences to quantify the effect of exogenous B-IAP protein on caspase activity. We found that cleavage activity matching the peptide preference of the initiator caspase (but not other peptides) was significantly reduced upon addition of B-IAP protein (Figure 4D), indicating that B-IAP functions as a potent inhibitor of planarian initiator caspases.

Together, our data indicate that B-IAP binds planarian initiator caspases and blocks their cleavage activity, thereby accomplishing an anti-apoptotic effect.

Burro1 is required for normal neoblast function and regeneration

Given the presence of the anti-apoptotic B-IAP protein in Burro1, we hypothesized that Burro1 might have a positive effect on planarian physiology. We used RNAi-mediated knockdown to

Please cite this article in press as: Lee et al., Host-transposon mutualism supports regeneration in planarians, Developmental Cell (2026), https://doi.org/10.1016/j.devcel.2026.03.001

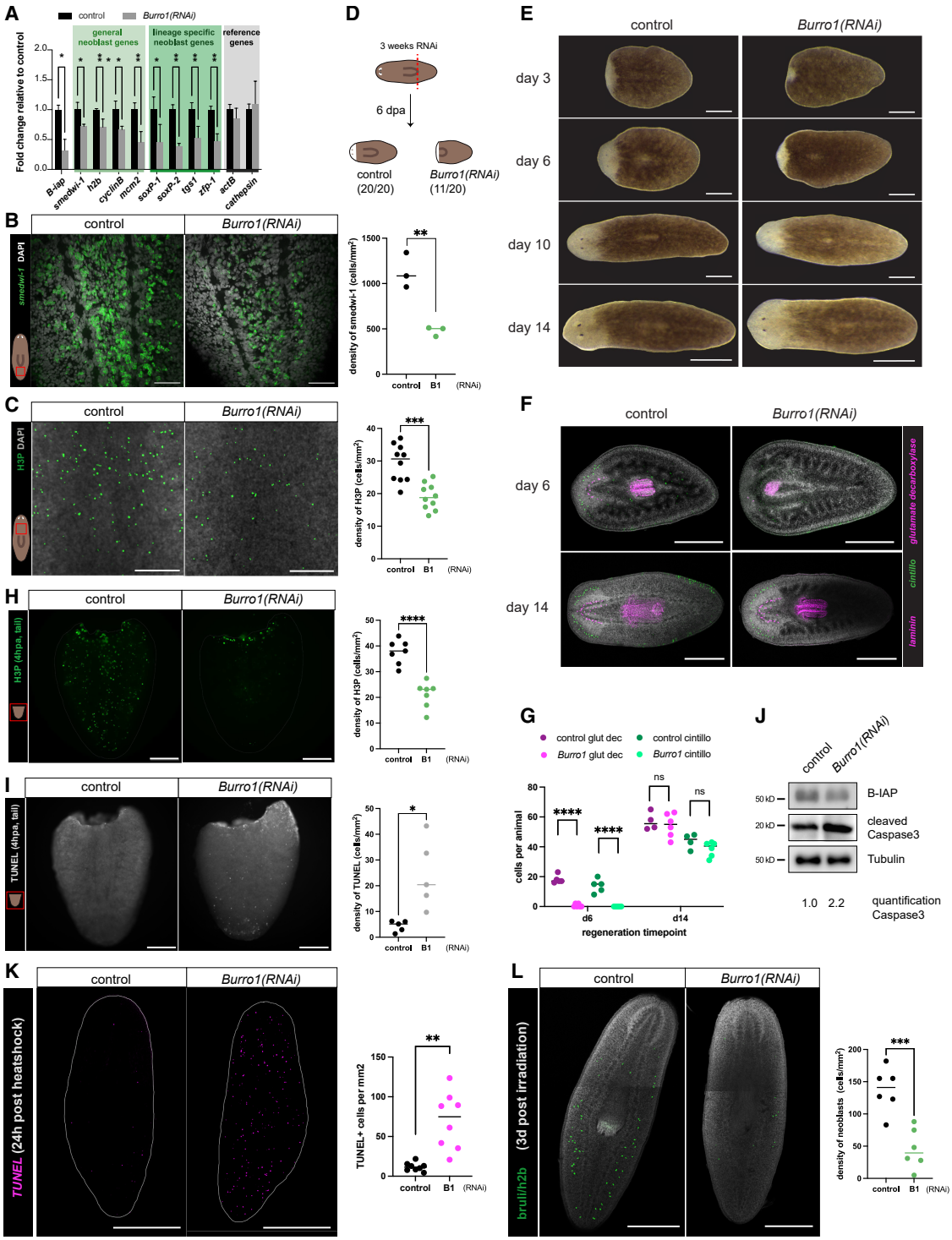

Figure 5. Burro1 supports regeneration in *S. mediterranea*

(A) qPCR quantification of transcript levels of several stem cell genes in *Burro1(RNAi)* samples compared with control RNAi. $n = 3$ samples of 2 animals each. Data are shown as mean ± SD.

(B) Representative images of FISH on whole-mount control animals and *Burro1(RNAi)* animals showing the stem cell marker *smedwi-1* (green). Right: quantification of the images. Scale bar, 50 μm. $n = 3$ individual animals per condition.

(C) Representative images of immunostaining on whole-mount control animals and *Burro1(RNAi)* animals showing the mitotic cell marker H3P (phosphorylated histone 3; green). Right: quantification of the images. Scale bar, 500 μm. $n = 10$ individual animals per condition.

(D) Schematic of the head regeneration experiment in control animals and *Burro1(RNAi)* animals at 6 days after amputation.

(legend continued on next page)

Please cite this article in press as: Lee et al., Host-transposon mutualism supports regeneration in planarians, Developmental Cell (2026), https://doi.org/10.1016/j.devcel.2026.03.001

obtain a significant reduction in *B-iap* transcript levels without affecting the genomic IAPs or other Burro transposons (Figures S5A and S5B). This resulted in a reduction in B-IAP protein (Figure 2D) and caused a moderate but significant reduction in the transcript levels of several stem cell (neoblast) genes (Figures 5A and S5A). FISH for the neoblast marker *smedwi-1* (Figure 5B), together with quantification of mitotic cells labeled by phosphorylated histone 3 (H3P) (Figure 5C), confirmed this reduction in the number of neoblasts in *Burro1(RNAi)* animals.

To assess the functional relevance of this neoblast reduction, we measured the regenerative response following head amputation. Head regeneration was significantly delayed in *Burro1(RNAi)* animals compared with controls (Figures 5D and 5E). FISH analysis of anterior neuronal and pharyngeal markers (*cintillo*, *glutamate decarboxylase*, and *laminin*, respectively) revealed both fewer anterior neuronal cells and a less developed pharynx in the *Burro1(RNAi)* animals at 6 days post amputation (Figures 5F and 5G). Despite this initial delay, regeneration eventually proceeded and by 14 days *Burro1(RNAi)* animals had largely completed the process.

The early response to tissue amputation typically involves localized apoptosis at the wound site combined with a systemic increase in mitosis, followed 2 days later by increased local mitosis at the wound site to regenerate the missing tissue.[58,59] However, upon reduction of B-IAP, we observed a subdued early mitotic activation, as marked by H3P (Figure 5H), alongside a significant increase in apoptotic bodies detected by TUNEL (Terminal deoxynucleotidyl transferase dUTP nick end labeling) (Figure 5I). Apoptosis extended throughout the parenchymal region, where the neoblasts reside, suggesting that the increased apoptosis in the absence of B-IAP may have caused the observed regeneration delay. Interestingly, knocking down caspase_9038 had the opposite effect, modestly accelerating regeneration. This was most evident on day 6 post amputation when *caspase_9038(RNAi)* animals had a fully formed pharynx and mouth, whereas the pharynx of control animals remained underdeveloped and disconnected from the ventral surface (Figure S5C). Furthermore, knockdown of *caspase_9038* largely rescued the regeneration phenotype of *Burro1(RNAi)* animals (Figure S5D), indicating that the *Burro1(RNAi)* regeneration delay was likely driven by overactivity of the caspase. To further verify the impact of B-IAP on the level of apoptosis during regeneration, we quantified activated (cleaved) caspase-3 upon amputation by western blot (Figure 5J) and indeed detected a significant increase in the level of cleaved caspase in the absence of B-IAP, indicating increased apoptotic activity.

We tested the physiological responses to several other stress conditions to assess whether the protective effect of Burro1 extended to these conditions. We found that heat stress resulted in a modest level of apoptotic cells in control animals, but in *Burro1(RNAi)* animals the density of apoptotic cells was significantly increased (Figures 5K and S5E). Furthermore, we found that a dose of irradiation that consistently left a considerable number of neoblasts in controls resulted in a significantly stronger loss of neoblasts in the *Burro1(RNAi)* animals (Figure 5L), whereas *caspase(RNAi)* animals exhibited the inverse effect (Figures S5F and S5G).

Together, our findings show that the active giant transposon Burro1 expresses a functional anti-apoptotic protein that protects planarian stem cells from apoptosis and enhances their regenerative abilities. This is a striking example of mutualism between a transposon and its eukaryote host and provides an exciting model for how transposons can positively impact the fitness of their host.

DISCUSSION

The interaction between transposons and their hosts has often been described as an arms race, in which the host is best served by the inactivation or elimination of the transposon. While this is probably true for most transposons, we here describe a different collaborative strategy between transposon and host—one that supports maintenance of the transposon *and* benefits the host. We find that the giant retrotransposon Burro1 includes a sequence encoding the BIR-domain protein B-IAP that was derived from its host. B-IAP has retained its function as an anti-apoptotic protein that inhibits the activation of host caspases, but its expression has become stress responsive. This provides stem cells carrying Burro1 with increased stress resistance and enhances host regeneration, albeit at the cost of higher transcriptional noise and the inherent risks of mobilization. It appears that this trade-off results in the positive selection of cells with Burro1, aiding the maintenance and expansion of this transposon.

(E) Representative live images of regenerating tail pieces of control animals and *Burro1(RNAi)* animals at indicated time points after amputation. Scale bar, 1 mm. $n = 8$ individual animals per condition.

(F) Representative images of FISH for anterior neuronal markers *cintillio* (magenta) and *glutamate decarboxylase* (green), and the pharynx marker *laminin*, in regenerating tail pieces of control animals and *Burro1(RNAi)* animals at the indicated time points after amputation. Scale bar, 500 μm. $n = 5$ individual animals for day 6 time points; 4 animals for day 14 controls, and 6 animals for day 14 *Burro1(RNAi)*.

(G) Quantification of the neuronal markers shown in (F).

(H) Representative images of immunostaining on tail pieces of control animals and *Burro1(RNAi)* animals showing the mitotic cell marker H3P (green) 4 h after amputation. Right: quantification of the images. Scale bar, 200 μm. $n = 7$ individual animals per condition.

(I) Representative image of TUNEL staining on tail pieces from control and *Burro1(RNAi)* animals 4 h after amputation, showing increased apoptosis upon knockdown of Burro1. Right: quantification of the images. Scale bar, 200 μm. $n = 5$ individual animals per condition.

(J) Western blot showing the level of activated caspase-3 in control animals and *Burro1(RNAi)* animals 4 h after amputation. Quantification is relative to the tubulin signal.

(K) Representative image (tile scan) of TUNEL staining on control and *Burro1(RNAi)* animals 1 day after heat stress, showing increased apoptosis upon knockdown of Burro1. Right: quantification of the images. Scale bar, 300 μm. $n = 8$ individual animals per condition.

(L) Representative image (tile scan) of FISH staining for neoblast markers (*bruli* and *h2b*) in control and *Burro1(RNAi)* animals 3 days after 1,250 Rads of irradiation, showing reduced neoblast survival in the *Burro1(RNAi)* animals. Right: quantification of the images. Scale bar, 500 μm. $n = 6$ individual animals per condition. Significance in (A)–(C), (G)–(I), (K), and (L) is $^{*}p \leq 0.05$, $^{**}p \leq 0.01$, $^{***}p \leq 0.001$, and $^{****}p \leq 0.0001$ by Student's *t* test.

See also Figure S5.

Please cite this article in press as: Lee et al., Host-transposon mutualism supports regeneration in planarians, Developmental Cell (2026), https://doi.org/10.1016/j.devcel.2026.03.001

Capture of non-transposon ORFs has previously been observed in retroviruses[65] and in retrotransposons in rotifers and plants.[66–68] Some of these ORFs resemble endoviral envelope (ENV) proteins and may enable horizontal spreading. Most accessory ORFs, however, lack similarity to any known genes, and their role in transposon survival or host interaction has thus remained unresolved. In the case of B-IAP, however, recognizable domains pointed to a specific function in apoptosis, and we were therefore able to establish that this transposon-captured protein directly and impactfully alters the biology of its host cell.

The connection between retrotransposons and the regulation of apoptosis has also been noted in several other contexts. Gene duplications introduced by retrotransposons resulted in the massive expansion of p53 gene copies in large mammals.[69] In gibbons, a retrotransposon was found to provide enhancers to several genes involved in DNA break repair,[70] and throughout mammalian genomes, IAP family genes have acquired enhancer elements from retrotransposons.[71] Finally, in oysters and clams, IAP elements have dramatically expanded in the genome, in part through the action of retrotransposons.[72,73] These observations raise the possibility that transposons may have repeatedly evolved the ability to modulate the level of apoptosis in their hosts. It is possible that transcriptional noise or DNA damage induced by some transposons is so significant that suppressing host apoptosis becomes an essential survival strategy for these elements themselves, although the modest activity of most extant elements may argue against this. Regardless, these findings make a strong argument for investigating whether other accessory ORFs with currently unknown homology also function as apoptotic modulators.

We find that transcription of *b-iap* is activated upon stress, including immediately after wounding, resulting in enhanced regeneration of the planarian host. Interestingly, transposable elements have been linked to the process of regeneration in several other highly regenerative animals. In hydra, axolotl, newt, and sea cucumber, transposons were upregulated upon injury.[74–77] An intriguing possibility is that a transient release of transposon silencing serves to prime defenses against related elements, as proposed for some transposon activation events during development.[78–81] In sea cucumber, it was noted that although apoptosis around the wound site was prominent, the transposon-expressing cells survived and contributed to regenerated tissues, suggesting that transposon expression could confer a protective benefit.[75] A recent earthworm genome assembly revealed that genes expressed during regeneration tended to be associated with transposable elements.[82] Together, these findings suggest the widespread activation of transposons upon wounding in regenerative animals, which may render them ideally positioned to contribute elements that enhance the cellular stress response.

The notion that Burro1 may have enhanced the regenerative capabilities of planarians is enticing. While our lack of data regarding the regenerative abilities of the Burro-less ancestor makes it difficult to prove this definitively, the distribution of regenerative abilities among extant planarians provides some support. Most planarians can regenerate, yet the *Dugesiidae* (which is the main clade carrying the Burro transposon) exhibit substantially improved regenerative abilities compared with other planarian families.[83] Closer inspection of *Dugesiidae* transcriptomes revealed that all contain a Burro-related Ty3 sequence and multiple copies of *iap-2*/*B-iap*. Although *B-iap* and *iap-2* sequences are difficult to distinguish phylogenetically, the co-occurrence of a Burro-like Ty3 sequence with multiple copies of the *iap-2*/*B-iap* sequence makes it highly probable that Burro1 is present and transcribed throughout this clade. Interestingly, *Cura pinguis*, the only known species in this clade with more limited regeneration, contains a Burro-like Ty3 element but lacks a second *iap-2* like sequence, suggesting that its Burro1 may be incomplete. In contrast, the *Planariidae* clade, which exhibits intermediate regenerative abilities, lacks Burro-related sequences entirely. However, we found that the robustly regenerating species in this group[83] all encode multiple copies of the *iap-1* gene, a unique feature of this clade. While there certainly are many other differences in genomic makeup among these planarian clades, these observations raise the possibility that expansion of *iap* copy number enhances regeneration and that Burro1 facilitated this process in *Dugesiidae*.

Transposon mutualisms are probably rare, and they may be prone to dissolve into parasitism through loss of the benefit provided by the transposon or into domestication by bringing the beneficial element under host control.[84,85] There may, however, be a benefit to retaining *B-iap* on an active mobile element rather than as a domesticated gene. First, transposable elements have long been proposed to activate under stress.[86–88] The presence of the anti-apoptotic *B-iap* on a transposon thus ensures activation of the gene when it is most needed without requiring recruitment of a specific promoter. Second, under persistent stress, sustained elevated expression of Burro1 will likely result in new Burro1 insertions, thereby dynamically increasing *B-iap* gene dosage and the stress resistance of host cells when the environmental conditions demand it, potentially generating heterogeneity among the existing cells to optimize the dose. This may be particularly important for long-lived cells, such as planarian neoblasts, which could thereby acquire an additional mechanism of adaptation to changing conditions.

The existence of beneficial interactions with transposons may also impact the evolution of host defense mechanisms. The primary eukaryotic defenses (PIWI interactig RNAs (piRNAs), small interfering RNAs (siRNAs), and Kruppel-associated box Zinc fingers (KRAB-ZNFs)) are sequence specific and thus target each transposon individually. This specificity may allow the host to titrate its defensive response based on the benefit provided by each particular element. By uncovering mutualistic features within a eukaryote mobile element, our study reveals an unexpected alliance between transposon and host and enhances our appreciation of the intricate interplay among transposons, host defense systems, and the trajectory of genome evolution.

Limitations of the study

To study the effect of the B-IAP protein on planarian physiology, we used RNAi to knock down the Burro1 transcript. This results in a reduction of B-IAP protein levels but residual protein remains. The effect of full elimination of B-IAP may therefore be stronger than the effects reported in this study. Furthermore, because *B-iap* is part of the Burro1 transcript, we are unable to separate the effects of knockdown of the B-IAP protein from potential effects from the rest of the Burro1 transposon, and the

effect of the presence of the *B-iap* sequence on Burro1 propagation efficiency cannot be explicitly tested.

Models regarding the origin of Burro1 and the evolutionary effect of Burro1 in platyhelminths are based on data of extant species and therefore remain inferential.

RESOURCE AVAILABILITY

Lead contact

Requests for further information and resources should be directed to and will be fulfilled by the lead contact, J.C. van Wolfswinkel (josien.van.wolfswinkel@yale.edu).

Materials availability

All unique/stable reagents generated in this study are available from the lead contact without restriction.

Data and code availability

- Sequencing data have been deposited in the SRA under accession number SRA: PRJNA1135975 and are publicly available as of the date of publication. This paper analyzes existing, publicly available data accessible under accession numbers SRA: PRJNA276084 and SRA: PRJNA1011852
- Raw western blots have been deposited on Mendeley Data: https://doi.org/10.17632/8gk5ssdtvp.1.
- This paper does not report original code.
- Any additional information required to reanalyze the data reported in this paper is available from the lead contact upon request.

ACKNOWLEDGMENTS

We thank Dr. David Schatz and members of the van Wolfswinkel lab for support and discussion. We are grateful to the Keck DNA Sequencing Facility and the MS & Proteomics Resource at Yale University for services provided.

This work was supported by NIH grants R01AG078926 and R35GM158281 (to J.C.v.W.).

AUTHOR CONTRIBUTIONS

Conceptualization, H.-L.L. and J.C.v.W.; funding acquisition, J.C.v.W.; supervision, J.C.v.W.; investigation and analysis, H.-L.L. and S.A.P.; methodology, H.-L.L. and J.C.v.W.; formal analysis and software, H.-L.L. and A.P.; writing—original draft, J.C.v.W.; writing—review and editing, H.-L.L., S.A.P., A.P., and J.C.v.W.

DECLARATION OF INTERESTS

The authors declare no competing interests.

STAR★METHODS

Detailed methods are provided in the online version of this paper and include the following:

- KEY RESOURCES TABLE
- EXPERIMENTAL MODEL AND STUDY PARTICIPANT DETAILS
  - Planarian strain and husbandry
  - Cell culture
- METHOD DETAILS
  - RNAi and drug treatment
  - Stress conditions
  - Whole-mount fluorescent in situ hybridization and immunofluorescence
  - Neoblast isolation and staining
  - Microscopy and image analysis
  - qPCR analysis
  - Polysome profiling
  - Nanopore sequencing and 5'RACE
  - In vitro caspase assays
  - Protein structure predictions
  - *In vitro* interaction assays
  - B-IAP antibody generation
  - SDS-PAGE and Western blotting
  - Phylogenetic analysis
  - Processing of mRNA-seq data
- QUANTIFICATION AND STATISTICAL ANALYSIS

SUPPLEMENTAL INFORMATION

Supplemental information can be found online at https://doi.org/10.1016/j.devcel.2026.03.001.

Received: November 13, 2025
Revised: January 15, 2026
Accepted: March 3, 2026

REFERENCES

1. Sotero-Caio, C.G., Platt, R.N., 2nd, Suh, A., and Ray, D.A. (2017). Evolution and Diversity of Transposable Elements in Vertebrate Genomes. Genome Biol. Evol. *9*, 161–177. https://doi.org/10.1093/gbe/evw264.
2. Schnable, P.S., Ware, D., Fulton, R.S., Stein, J.C., Wei, F., Pasternak, S., Liang, C., Zhang, J., Fulton, L., Graves, T.A., et al. (2009). The B73 maize genome: complexity, diversity, and dynamics. Science *326*, 1112–1115. https://doi.org/10.1126/science.1178534.
3. Orgel, L.E., and Crick, F.H. (1980). Selfish DNA: the ultimate parasite. Nature *284*, 604–607. https://doi.org/10.1038/284604a0.
4. Doolittle, W.F., and Sapienza, C. (1980). Selfish genes, the phenotype paradigm and genome evolution. Nature *284*, 601–603. https://doi.org/10.1038/284601a0.
5. McClintock, B. (1950). The origin and behavior of mutable loci in maize. Proc. Natl. Acad. Sci. USA *36*, 344–355. https://doi.org/10.1073/pnas.36.6.344.
6. Cosby, R.L., Chang, N.C., and Feschotte, C. (2019). Host-transposon interactions: conflict, cooperation, and cooption. Genes Dev. *33*, 1098–1116. https://doi.org/10.1101/gad.327312.119.
7. Bergstrom, C.T., Lipsitch, M., and Levin, B.R. (2000). Natural selection, infectious transfer and the existence conditions for bacterial plasmids. Genetics *155*, 1505–1519. https://doi.org/10.1093/genetics/155.4.1505.
8. Eberhard, W.G. (1990). Evolution in bacterial plasmids and levels of selection. Q. Rev. Biol. *65*, 3–22. https://doi.org/10.1086/416582.
9. Nuti, M.P., Lepidi, A.A., Prakash, R.K., Schilperoort, R.A., and Cannon, F.C. (1979). Evidence for Nitrogen Fixation (Nif) Genes on Indigenous Rhizobium Plasmids. Nature *282*, 533–535. https://doi.org/10.1038/282533a0.
10. Martínez, J.L. (2008). Antibiotics and antibiotic resistance genes in natural environments. Science *321*, 365–367. https://doi.org/10.1126/science.1159483.
11. Ross, K., Varani, A.M., Snesrud, E., Huang, H., Alvarenga, D.O., Zhang, J., Wu, C., McGann, P., and Chandler, M. (2021). TnCentral: a Prokaryotic Transposable Element Database and Web Portal for Transposon Analysis. mBio *12*, e0206021. https://doi.org/10.1128/mBio.02060-21.
12. Wagner, A. (2006). Cooperation is fleeting in the world of transposable elements. PLoS Comput. Biol. *2*, e162. https://doi.org/10.1371/journal.pcbi.0020162.
13. Bourque, G., Burns, K.H., Gehring, M., Gorbunova, V., Seluanov, A., Hammell, M., Imbeault, M., Izsvák, Z., Levin, H.L., Macfarlan, T.S.,

et al. (2018). Ten things you should know about transposable elements. Genome Biol. *19*, 199. https://doi.org/10.1186/s13059-018-1577-z.

14. Levis, R.W., Ganesan, R., Houtchens, K., Tolar, L.A., and Sheen, F.M. (1993). Transposons in place of telomeric repeats at a Drosophila telomere. Cell *75*, 1083–1093. https://doi.org/10.1016/0092-8674(93)90318-k.
15. Kursel, L.E., and Malik, H.S. (2016). Centromeres. Curr. Biol. *26*, R487–R490. https://doi.org/10.1016/j.cub.2016.05.031.
16. Wong, L.H., and Choo, K.H.A. (2004). Evolutionary dynamics of transposable elements at the centromere. Trends Genet. *20*, 611–616. https://doi.org/10.1016/j.tig.2004.09.011.
17. Diehl, A.G., Ouyang, N., and Boyle, A.P. (2020). Transposable elements contribute to cell and species-specific chromatin looping and gene regulation in mammalian genomes. Nat. Commun. *11*, 1796. https://doi.org/10.1038/s41467-020-15520-5.
18. Choudhary, M.N., Friedman, R.Z., Wang, J.T., Jang, H.S., Zhuo, X., and Wang, T. (2020). Co-opted transposons help perpetuate conserved higher-order chromosomal structures. Genome Biol. *21*, 16. https://doi.org/10.1186/s13059-019-1916-8.
19. Fuentes, D.R., Swigut, T., and Wysocka, J. (2018). Systematic perturbation of retroviral LTRs reveals widespread long-range effects on human gene regulation. eLife *7*, e35989. https://doi.org/10.7554/eLife.35989.
20. Jachowicz, J.W., Bing, X., Pontabry, J., Bošković, A., Rando, O.J., and Torres-Padilla, M.E. (2017). LINE-1 activation after fertilization regulates global chromatin accessibility in the early mouse embryo. Nat. Genet. *49*, 1502–1510. https://doi.org/10.1038/ng.3945.
21. Sasaki, T., Nishihara, H., Hirakawa, M., Fujimura, K., Tanaka, M., Kokubo, N., Kimura-Yoshida, C., Matsuo, I., Sumiyama, K., Saitou, N., et al. (2008). Possible involvement of SINEs in mammalian-specific brain formation. Proc. Natl. Acad. Sci. USA *105*, 4220–4225. https://doi.org/10.1073/pnas.0709398105.
22. Lynch, V.J., Leclerc, R.D., May, G., and Wagner, G.P. (2011). Transposon-mediated rewiring of gene regulatory networks contributed to the evolution of pregnancy in mammals. Nat. Genet. *43*, 1154–1159. https://doi.org/10.1038/ng.917.
23. Lynch, V.J., Nnamani, M.C., Kapusta, A., Brayer, K., Plaza, S.L., Mazur, E.C., Emera, D., Sheikh, S.Z., Grützner, F., Bauersachs, S., et al. (2015). Ancient transposable elements transformed the uterine regulatory landscape and transcriptome during the evolution of mammalian pregnancy. Cell Rep. *10*, 551–561. https://doi.org/10.1016/j.celrep.2014.12.052.
24. Fueyo, R., Judd, J., Feschotte, C., and Wysocka, J. (2022). Roles of transposable elements in the regulation of mammalian transcription. Nat. Rev. Mol. Cell Biol. *23*, 481–497. https://doi.org/10.1038/s41580-022-00457-y.
25. Casola, C., Hucks, D., and Feschotte, C. (2008). Convergent domestication of pogo-like transposases into centromere-binding proteins in fission yeast and mammals. Mol. Biol. Evol. *25*, 29–41. https://doi.org/10.1093/molbev/msm221.
26. Chuong, E.B., Elde, N.C., and Feschotte, C. (2016). Regulatory evolution of innate immunity through co-option of endogenous retroviruses. Science *351*, 1083–1087. https://doi.org/10.1126/science.aad5497.
27. Mi, S., Lee, X., Li, X., Veldman, G.M., Finnerty, H., Racie, L., LaVallie, E., Tang, X.Y., Edouard, P., Howes, S., et al. (2000). Syncytin is a captive retroviral envelope protein involved in human placental morphogenesis. Nature *403*, 785–789. https://doi.org/10.1038/35001608.
28. Emerson, R.O., and Thomas, J.H. (2011). Gypsy and the birth of the SCAN domain. J. Virol. *85*, 12043–12052. https://doi.org/10.1128/JVI.00867-11.
29. Brandt, J., Schrauth, S., Veith, A.M., Froschauer, A., Haneke, T., Schultheis, C., Gessler, M., Leimeister, C., and Volff, J.N. (2005). Transposable elements as a source of genetic innovation: expression and evolution of a family of retrotransposon-derived neogenes in mammals. Gene *345*, 101–111. https://doi.org/10.1016/j.gene.2004.11.022.
30. Belfort, M., Curcio, M.J., and Lue, N.F. (2011). Telomerase and retrotransposons: reverse transcriptases that shaped genomes. Proc. Natl. Acad. Sci. USA *108*, 20304–20310. https://doi.org/10.1073/pnas.1100269109.
31. Modzelewski, A.J., Gan Chong, J., Wang, T., and He, L. (2022). Mammalian genome innovation through transposon domestication. Nat. Cell Biol. *24*, 1332–1340. https://doi.org/10.1038/s41556-022-00970-4.
32. Trizzino, M., Park, Y., Holsbach-Beltrame, M., Aracena, K., Mika, K., Caliskan, M., Perry, G.H., Lynch, V.J., and Brown, C.D. (2017). Transposable elements are the primary source of novelty in primate gene regulation. Genome Res. *27*, 1623–1633. https://doi.org/10.1101/gr.218149.116.
33. Kapitonov, V.V., and Jurka, J. (2005). RAG1 core and V(D)J recombination signal sequences were derived from Transib transposons. PLoS Biol. *3*, e181. https://doi.org/10.1371/journal.pbio.0030181.
34. Agrawal, A., Eastman, Q.M., and Schatz, D.G. (1998). Transposition mediated by RAG1 and RAG2 and its implications for the evolution of the immune system. Nature *394*, 744–751. https://doi.org/10.1038/29457.
35. Nakamura, T.M., and Cech, T.R. (1998). Reversing time: origin of telomerase. Cell *92*, 587–590. https://doi.org/10.1016/s0092-8674(00)81123-x.
36. Cordaux, R., Udit, S., Batzer, M.A., and Feschotte, C. (2006). Birth of a chimeric primate gene by capture of the transposase gene from a mobile element. Proc. Natl. Acad. Sci. USA *103*, 8101–8106. https://doi.org/10.1073/pnas.0601161103.
37. Pardue, M.L., and DeBaryshe, P.G. (2003). Retrotransposons provide an evolutionarily robust non-telomerase mechanism to maintain telomeres. Annu. Rev. Genet. *37*, 485–511. https://doi.org/10.1146/annurev.genet.38.072902.093115.
38. Nelson, J.O., Slicko, A., and Yamashita, Y.M. (2023). The retrotransposon R2 maintains Drosophila ribosomal DNA repeats. Proc. Natl. Acad. Sci. USA *120*, e2221613120. https://doi.org/10.1073/pnas.2221613120.
39. Percharde, M., Lin, C.J., Yin, Y., Guan, J., Peixoto, G.A., Bulut-Karslioglu, A., Biechele, S., Huang, B., Shen, X., and Ramalho-Santos, M. (2018). A LINE1-Nucleolin Partnership Regulates Early Development and ESC Identity. Cell *174*, 391–405.e19. https://doi.org/10.1016/j.cell.2018.05.043.
40. Sakashita, A., Kitano, T., Ishizu, H., Guo, Y., Masuda, H., Ariura, M., Murano, K., and Siomi, H. (2023). Transcription of MERVL retrotransposons is required for preimplantation embryo development. Nat. Genet. *55*, 484–495. https://doi.org/10.1038/s41588-023-01324-y.
41. Grohme, M.A., Schloissnig, S., Rozanski, A., Pippel, M., Young, G.R., Winkler, S., Brandl, H., Henry, I., Dahl, A., Powell, S., et al. (2018). The genome of Schmidtea mediterranea and the evolution of core cellular mechanisms. Nature *554*, 56–61. https://doi.org/10.1038/nature25473.
42. Arkhipova, I.R., and Yushenova, I.A. (2019). Giant Transposons in Eukaryotes: Is Bigger Better? Genome Biol. Evol. *11*, 906–918. https://doi.org/10.1093/gbe/evz041.
43. Jurka, J. (2007). GYPSM1: Gypsy-type sequence from freshwater planarian (Schmidtea mediterranea). Repbase Rep. *7*, 186.
44. Kimura, M. (1980). A simple method for estimating evolutionary rates of base substitutions through comparative studies of nucleotide sequences. J. Mol. Evol. *16*, 111–120. https://doi.org/10.1007/BF01731581.
45. Sol, E., Sluys, R., Riutort, M., and Kawakatsu, M. (2023). Molecular phylogenetics facilitates the first historical biogeographic analysis of the hammerhead worms (Platyhelminthes: Tricladida: Bipaliinae), with the description of twelve new species and two new genera. Zootaxa *5335*, 1–77. https://doi.org/10.11646/zootaxa.5335.1.1.
46. Sluys, R. (2019). The evolutionary terrestrialization of planarian flatworms (Platyhelminthes, Tricladida, Geoplanidae): a review and research programme. Zoosyst. Evol. *95*, 543–556. https://doi.org/10.3897/zse.95.38727.
47. Blumenstiel, J.P. (2019). Birth, School, Work, Death, and Resurrection: The Life Stages and Dynamics of Transposable Element Proliferation. Genes (Basel) *10*, 336. https://doi.org/10.3390/genes10050336.

48. Le Rouzic, A., Boutin, T.S., and Capy, P. (2007). Long-term evolution of transposable elements. Proc. Natl. Acad. Sci. USA *104*, 19375–19380. https://doi.org/10.1073/pnas.0705238104.

49. Capy, P. (2021). Taming, Domestication and Exaptation: Trajectories of Transposable Elements in Genomes. Cells *10*, 3590. https://doi.org/10.3390/cells10123590.

50. SanMiguel, P., Gaut, B.S., Tikhonov, A., Nakajima, Y., and Bennetzen, J.L. (1998). The paleontology of intergene retrotransposons of maize. Nat. Genet. *20*, 43–45. https://doi.org/10.1038/1695.

51. Ziman, B., Barghouth, P.G., Maciel, E.I., and Oviedo, N.J. (2020). TRAF-like Proteins Regulate Cellular Survival in the Planarian Schmidtea mediterranea. iScience *23*, 101665. https://doi.org/10.1016/j.isci.2020.101665.

52. Yang, Y.L., and Li, X.M. (2000). The IAP family: endogenous caspase inhibitors with multiple biological activities. Cell Res. *10*, 169–177. https://doi.org/10.1038/sj.cr.7290046.

53. Cao, L., Wang, Z., Yang, X., Xie, L., and Yu, L. (2008). The evolution of BIR domain and its containing proteins. FEBS Lett. *582*, 3817–3822. https://doi.org/10.1016/j.febslet.2008.09.058.

54. Li, D., Taylor, D.H., and van Wolfswinkel, J.C. (2021). PIWI-mediated control of tissue-specific transposons is essential for somatic cell differentiation. Cell Rep. *37*, 109776. https://doi.org/10.1016/j.celrep.2021.109776.

55. Allikka Parambil, S., Li, D., Zelko, M., Poulet, A., and van Wolfswinkel, J.C. (2024). piRNA generation is associated with the pioneer round of translation in stem cells. Nucleic Acids Res. *52*, 2590–2608. https://doi.org/10.1093/nar/gkad1212.

56. Fincher, C.T., Wurtzel, O., de Hoog, T., Kravarik, K.M., and Reddien, P.W. (2018). Cell type transcriptome atlas for the planarian Schmidtea mediterranea. Science *360*, eaaq1736. https://doi.org/10.1126/science.aaq1736.

57. Wurtzel, O., Cote, L.E., Poirier, A., Satija, R., Regev, A., and Reddien, P.W. (2015). A Generic and Cell-Type-Specific Wound Response Precedes Regeneration in Planarians. Dev. Cell *35*, 632–645. https://doi.org/10.1016/j.devcel.2015.11.004.

58. Wenemoser, D., and Reddien, P.W. (2010). Planarian regeneration involves distinct stem cell responses to wounds and tissue absence. Dev. Biol. *344*, 979–991. https://doi.org/10.1016/j.ydbio.2010.06.017.

59. Pellettieri, J., Fitzgerald, P., Watanabe, S., Mancuso, J., Green, D.R., and Sánchez Alvarado, A. (2010). Cell death and tissue remodeling in planarian regeneration. Dev. Biol. *338*, 76–85. https://doi.org/10.1016/j.ydbio.2009.09.015.

60. Salvesen, G.S., and Duckett, C.S. (2002). IAP proteins: blocking the road to death's door. Nat. Rev. Mol. Cell Biol. *3*, 401–410. https://doi.org/10.1038/nrm830.

61. Silke, J., Ekert, P.G., Day, C.L., Hawkins, C.J., Baca, M., Chew, J., Pakusch, M., Verhagen, A.M., and Vaux, D.L. (2001). Direct inhibition of caspase 3 is dispensable for the anti-apoptotic activity of XIAP. EMBO J. *20*, 3114–3123. https://doi.org/10.1093/emboj/20.12.3114.

62. O'Riordan, M.X.D., Bauler, L.D., Scott, F.L., and Duckett, C.S. (2008). Inhibitor of apoptosis proteins in eukaryotic evolution and development: a model of thematic conservation. Dev. Cell *15*, 497–508. https://doi.org/10.1016/j.devcel.2008.09.012.

63. Scott, F.L., Denault, J.B., Riedl, S.J., Shin, H., Renatus, M., and Salvesen, G.S. (2005). XIAP inhibits caspase-3 and -7 using two binding sites: evolutionarily conserved mechanism of IAPs. EMBO J. *24*, 645–655. https://doi.org/10.1038/sj.emboj.7600544.

64. Eckelman, B.P., and Salvesen, G.S. (2006). The human anti-apoptotic proteins cIAP1 and cIAP2 bind but do not inhibit caspases. J. Biol. Chem. *281*, 3254–3260. https://doi.org/10.1074/jbc.M510863200.

65. Katz, R.A., and Skalka, A.M. (1990). Generation of diversity in retroviruses. Annu. Rev. Genet. *24*, 409–445. https://doi.org/10.1146/annurev.ge.24.120190.002205.

66. Rodriguez, F., Kenefick, A.W., and Arkhipova, I.R. (2017). LTR-Retrotransposons from Bdelloid Rotifers Capture Additional ORFs Shared between Highly Diverse Retroelement Types. Viruses *9*, 78. https://doi.org/10.3390/v9040078.

67. Steinbauerová, V., Neumann, P., Novák, P., and Macas, J. (2011). A widespread occurrence of extra open reading frames in plant Ty3/gypsy retrotransposons. Genetica *139*, 1543–1555. https://doi.org/10.1007/s10709-012-9654-9.

68. Vicient, C.M., and Casacuberta, J.M. (2020). Additional ORFs in Plant LTR-Retrotransposons. Front. Plant Sci. *11*, 555. https://doi.org/10.3389/fpls.2020.00555.

69. Sulak, M., Fong, L., Mika, K., Chigurupati, S., Yon, L., Mongan, N.P., Emes, R.D., and Lynch, V.J. (2016). TP53 copy number expansion is associated with the evolution of increased body size and an enhanced DNA damage response in elephants. eLife *5*, e11994. https://doi.org/10.7554/eLife.11994.

70. Okhovat, M., Nevonen, K.A., Davis, B.A., Michener, P., Ward, S., Milhaven, M., Harshman, L., Sohota, A., Fernandes, J.D., Salama, S.R., et al. (2020). Co-option of the lineage-specific LAVA retrotransposon in the gibbon genome. Proc. Natl. Acad. Sci. USA *117*, 19328–19338. https://doi.org/10.1073/pnas.2006038117.

71. Romanish, M.T., Lock, W.M., van de Lagemaat, L.N., Dunn, C.A., and Mager, D.L. (2007). Repeated recruitment of LTR retrotransposons as promoters by the anti-apoptotic locus NAIP during mammalian evolution. PLoS Genet. *3*, e10. https://doi.org/10.1371/journal.pgen.0030010.

72. Song, H., Guo, X., Sun, L., Wang, Q., Han, F., Wang, H., Wray, G.A., Davidson, P., Wang, Q., Hu, Z., et al. (2021). The hard clam genome reveals massive expansion and diversification of inhibitors of apoptosis in Bivalvia. BMC Biol. *19*, 15. https://doi.org/10.1186/s12915-020-00943-9.

73. Witkop, E.M., Proestou, D.A., and Gomez-Chiarri, M. (2022). The expanded inhibitor of apoptosis gene family in oysters possesses novel domain architectures and may play diverse roles in apoptosis following immune challenge. BMC Genomics *23*, 201. https://doi.org/10.1186/s12864-021-08233-6.

74. Zhu, W., Kuo, D., Nathanson, J., Satoh, A., Pao, G.M., Yeo, G.W., Bryant, S.V., Voss, S.R., Gardiner, D.M., and Hunter, T. (2012). Retrotransposon long interspersed nucleotide element-1 (LINE-1) is activated during salamander limb regeneration. Dev. Growth Differ. *54*, 673–685. https://doi.org/10.1111/j.1440-169X.2012.01368.x.

75. Mashanov, V.S., Zueva, O.R., and García-Arrarás, J.E. (2012). Posttraumatic regeneration involves differential expression of long terminal repeat (LTR) retrotransposons. Dev. Dyn. *241*, 1625–1636. https://doi.org/10.1002/dvdy.23844.

76. Elewa, A., Wang, H., Talavera-López, C., Joven, A., Brito, G., Kumar, A., Hameed, L.S., Penrad-Mobayed, M., Yao, Z., Zamani, N., et al. (2017). Reading and editing the Pleurodeles waltl genome reveals novel features of tetrapod regeneration. Nat. Commun. *8*, 2286. https://doi.org/10.1038/s41467-017-01964-9.

77. Petersen, H.O., Höger, S.K., Looso, M., Lengfeld, T., Kuhn, A., Warnken, U., Nishimiya-Fujisawa, C., Schnölzer, M., Krüger, M., Özbek, S., et al. (2015). A Comprehensive Transcriptomic and Proteomic Analysis of Hydra Head Regeneration. Mol. Biol. Evol. *32*, 1928–1947. https://doi.org/10.1093/molbev/msv079.

78. Svoboda, P., Stein, P., Anger, M., Bernstein, E., Hannon, G.J., and Schultz, R.M. (2004). RNAi and expression of retrotransposons MuERV-L and IAP in preimplantation mouse embryos. Dev. Biol. *269*, 276–285. https://doi.org/10.1016/j.ydbio.2004.01.028.

79. Wang, L., Tracy, L., Su, W., Yang, F., Feng, Y., Silverman, N., and Zhang, Z.Z.Z. (2022). Retrotransposon activation during Drosophila metamorphosis conditions adult antiviral responses. Nat. Genet. *54*, 1933–1945. https://doi.org/10.1038/s41588-022-01214-9.

80. Grow, E.J., Flynn, R.A., Chavez, S.L., Bayless, N.L., Wossidlo, M., Wesche, D.J., Martin, L., Ware, C.B., Blish, C.A., Chang, H.Y., et al. (2015). Intrinsic retroviral reactivation in human preimplantation embryos

and pluripotent cells. Nature *522*, 221–225. https://doi.org/10.1038/nature14308.

81. Ni, J.Z., Kalinava, N., Mendoza, S.G., and Gu, S.G. (2018). The spatial and temporal dynamics of nuclear RNAi-targeted retrotransposon transcripts in Caenorhabditis elegans. Development *145*, dev167346. https://doi.org/10.1242/dev.167346.

82. Shao, Y., Wang, X.B., Zhang, J.J., Li, M.L., Wu, S.S., Ma, X.Y., Wang, X., Zhao, H.F., Li, Y., Zhu, H.H., et al. (2020). Genome and single-cell RNA-sequencing of the earthworm Eisenia andrei identifies cellular mechanisms underlying regeneration. Nat. Commun. *11*, 2656. https://doi.org/10.1038/s41467-020-16454-8.

83. Vila-Farré, M., Rozanski, A., Ivanković, M., Cleland, J., Brand, J.N., Sandberg, F., Grohme, M.A., von Kannen, S., Grosbusch, A.L., Vu, H.T.K., et al. (2023). Evolutionary dynamics of whole-body regeneration across planarian flatworms. Nat. Ecol. Evol. *7*, 2108–2124. https://doi.org/10.1038/s41559-023-02221-7.

84. Sachs, J.L., and Simms, E.L. (2006). Pathways to mutualism breakdown. Trends Ecol. Evol. *21*, 585–592. https://doi.org/10.1016/j.tree.2006.06.018.

85. Toby Kiers, E., Palmer, T.M., Ives, A.R., Bruno, J.F., and Bronstein, J.L. (2010). Mutualisms in a changing world: an evolutionary perspective. Ecol. Lett. *13*, 1459–1474. https://doi.org/10.1111/j.1461-0248.2010.01538.x.

86. McClintock, B. (1984). The significance of responses of the genome to challenge. Science *226*, 792–801. https://doi.org/10.1126/science.15739260.

87. Wessler, S.R. (1996). Turned on by stress. Plant retrotransposons. Curr. Biol. *6*, 959–961. https://doi.org/10.1016/s0960-9822(02)00638-3.

88. Ratner, V.A., Zabanov, S.A., Kolesnikova, O.V., and Vasilyeva, L.A. (1992). Induction of the mobile genetic element Dm-412 transpositions in the Drosophila genome by heat shock treatment. Proc. Natl. Acad. Sci. USA *89*, 5650–5654. https://doi.org/10.1073/pnas.89.12.5650.

89. Ivanković, M., Brand, J.N., Pandolfini, L., Brown, T., Pippel, M., Rozanski, A., Schubert, T., Grohme, M.A., Winkler, S., Robledillo, L., et al. (2024). A comparative analysis of planarian genomes reveals regulatory conservation in the face of rapid structural divergence. Nat. Commun. *15*, 8215. https://doi.org/10.1038/s41467-024-52380-9.

90. Rozanski, A., Moon, H., Brandl, H., Martín-Durán, J.M., Grohme, M.A., Hüttner, K., Bartscherer, K., Henry, I., and Rink, J.C. (2019). PlanMine 3.0-improvements to a mineable resource of flatworm biology and biodiversity. Nucleic Acids Res. *47*, D812–D820. https://doi.org/10.1093/nar/gky1070.

91. An, Y., Kawaguchi, A., Zhao, C., Toyoda, A., Sharifi-Zarchi, A., Mousavi, S.A., Bagherzadeh, R., Inoue, T., Ogino, H., Fujiyama, A., et al. (2018). Draft genome of Dugesia japonica provides insights into conserved regulatory elements of the brain restriction gene nou-darake in planarians. Zool. Lett. *4*, 24. https://doi.org/10.1186/s40851-018-0102-2.

92. Fu, B., Li, S., Wang, L., Berman, M.A., and Dorf, M.E. (2014). The ubiquitin conjugating enzyme UBE2L3 regulates TNFalpha-induced linear ubiquitination. Cell Res. *24*, 376–379. https://doi.org/10.1038/cr.2013.133.

93. Yang, Y., Fang, S.Y., Jensen, J.P., Weissman, A.M., and Ashwell, J.D. (2000). Ubiquitin protein ligase activity of IAPs and their degradation in proteasomes in response to apoptotic stimuli. Science *288*, 874–877. https://doi.org/10.1126/science.288.5467.874.

94. Smit, A., Hubley, R., and Green, P. (2015). RepeatMasker Open-4.0. https://www.repeatmasker.org/.

95. Katoh, K., Rozewicki, J., and Yamada, K.D. (2019). MAFFT online service: multiple sequence alignment, interactive sequence choice and visualization. Brief. Bioinform. *20*, 1160–1166. https://doi.org/10.1093/bib/bbx108.

96. Tamura, K., Stecher, G., and Kumar, S. (2021). MEGA11: Molecular Evolutionary Genetics Analysis Version 11. Mol. Biol. Evol. *38*, 3022–3027. https://doi.org/10.1093/molbev/msab120.

97. Shen, W., Sipos, B., and Zhao, L. (2024). SeqKit2: A Swiss army knife for sequence and alignment processing. Imeta *3*, e191. https://doi.org/10.1002/imt2.191.

98. Rice, P., Longden, I., and Bleasby, A. (2000). EMBOSS: the European Molecular Biology Open Software Suite. Trends Genet. *16*, 276–277. https://doi.org/10.1016/s0168-9525(00)02024-2.

99. Camacho, C., Coulouris, G., Avagyan, V., Ma, N., Papadopoulos, J., Bealer, K., and Madden, T.L. (2009). BLAST+: architecture and applications. BMC Bioinform. *10*, 421. https://doi.org/10.1186/1471-2105-10-421.

100. Kozlov, A.M., Darriba, D., Flouri, T., Morel, B., and Stamatakis, A. (2019). RAxML-NG: a fast, scalable and user-friendly tool for maximum likelihood phylogenetic inference. Bioinformatics *35*, 4453–4455. https://doi.org/10.1093/bioinformatics/btz305.

101. Ronquist, F., Teslenko, M., van der Mark, P., Ayres, D.L., Darling, A., Höhna, S., Larget, B., Liu, L., Suchard, M.A., and Huelsenbeck, J.P. (2012). MrBayes 3.2: efficient Bayesian phylogenetic inference and model choice across a large model space. Syst. Biol. *61*, 539–542. https://doi.org/10.1093/sysbio/sys029.

102. Letunic, I., and Bork, P. (2024). Interactive Tree of Life (iTOL) v6: recent updates to the phylogenetic tree display and annotation tool. Nucleic Acids Res. *52*, W78–W82. https://doi.org/10.1093/nar/gkae268.

103. Frazer, K.A., Pachter, L., Poliakov, A., Rubin, E.M., and Dubchak, I. (2004). VISTA: computational tools for comparative genomics. Nucleic Acids Res. *32*, W273–W279. https://doi.org/10.1093/nar/gkh458.

104. Chen, S., Zhou, Y., Chen, Y., and Gu, J. (2018). fastp: an ultra-fast all-in-one FASTQ preprocessor. Bioinformatics *34*, i884–i890. https://doi.org/10.1093/bioinformatics/bty560.

105. Dobin, A., Davis, C.A., Schlesinger, F., Drenkow, J., Zaleski, C., Jha, S., Batut, P., Chaisson, M., and Gingeras, T.R. (2013). STAR: ultrafast universal RNA-seq aligner. Bioinformatics *29*, 15–21. https://doi.org/10.1093/bioinformatics/bts635.

106. Liao, Y., Smyth, G.K., and Shi, W. (2019). The R package Rsubread is easier, faster, cheaper and better for alignment and quantification of RNA sequencing reads. Nucleic Acids Res. *47*, e47. https://doi.org/10.1093/nar/gkz114.

107. Jumper, J., Evans, R., Pritzel, A., Green, T., Figurnov, M., Ronneberger, O., Tunyasuvunakool, K., Bates, R., Žídek, A., Potapenko, A., et al. (2021). Highly accurate protein structure prediction with AlphaFold. Nature *596*, 583–589. https://doi.org/10.1038/s41586-021-03819-2.

108. Liu, J., Guo, Z., Wu, T., Roy, R.S., Quadir, F., Chen, C., and Cheng, J. (2023). Enhancing alphafold-multimer-based protein complex structure prediction with MULTICOM in CASP15. Commun. Biol. *6*, 1140. https://doi.org/10.1038/s42003-023-05525-3.

109. Mirdita, M., Schütze, K., Moriwaki, Y., Heo, L., Ovchinnikov, S., and Steinegger, M. (2022). ColabFold: making protein folding accessible to all. Nat. Methods *19*, 679–682. https://doi.org/10.1038/s41592-022-01488-1.

110. Schindelin, J., Arganda-Carreras, I., Frise, E., Kaynig, V., Longair, M., Pietzsch, T., Preibisch, S., Rueden, C., Saalfeld, S., Schmid, B., et al. (2012). Fiji: an open-source platform for biological-image analysis. Nat. Methods *9*, 676–682. https://doi.org/10.1038/nmeth.2019.

111. Newmark, P.A., and Sánchez Alvarado, A. (2000). Bromodeoxyuridine specifically labels the regenerative stem cells of planarians. Dev. Biol. *220*, 142–153. https://doi.org/10.1006/dbio.2000.9645.

112. Rouhana, L., Weiss, J.A., Forsthoefel, D.J., Lee, H., King, R.S., Inoue, T., Shibata, N., Agata, K., and Newmark, P.A. (2013). RNA interference by feeding in vitro-synthesized double-stranded RNA to planarians: methodology and dynamics. Dev. Dyn. *242*, 718–730. https://doi.org/10.1002/dvdy.23950.

113. Pearson, B.J., Eisenhoffer, G.T., Gurley, K.A., Rink, J.C., Miller, D.E., and Sánchez Alvarado, A. (2009). Formaldehyde-based whole-mount *in situ* hybridization method for planarians. Dev. Dyn. *238*, 443–450. https://doi.org/10.1002/dvdy.21849.

114. King, R.S., and Newmark, P.A. (2013). In situ hybridization protocol for enhanced detection of gene expression in the planarian Schmidtea mediterranea. BMC Dev. Biol. *13*, 8. https://doi.org/10.1186/1471-213X-13-8.

115. Hayashi, T., Asami, M., Higuchi, S., Shibata, N., and Agata, K. (2006). Isolation of planarian X-ray-sensitive stem cells by fluorescence-activated cell sorting. Dev. Growth Differ. *48*, 371–380. https://doi.org/10.1111/j.1440-169X.2006.00876.x.

116. van Wolfswinkel, J.C., Wagner, D.E., and Reddien, P.W. (2014). Single-cell analysis reveals functionally distinct classes within the planarian stem cell compartment. Cell Stem Cell *15*, 326–339. https://doi.org/10.1016/j.stem.2014.06.007.

117. Guo, L., Bloom, J.S., Dols-Serrate, D., Boocock, J., Ben-David, E., Schubert, O.T., Kozuma, K., Ho, K., Warda, E., Chui, C., et al. (2022). Island-specific evolution of a sex-primed autosome in a sexual planarian. Nature *606*, 329–334. https://doi.org/10.1038/s41586-022-04757-3.

118. Panda, A.C., Martindale, J.L., and Gorospe, M. (2017). Polysome Fractionation to Analyze mRNA Distribution Profiles. Bio Protoc. *7*, e2126. https://doi.org/10.21769/BioProtoc.2126.

119. Xu, H., Mao, M., Zhao, R., and Zhao, Q. (2021). Enoxacin Exerts Anti-Tumor Effects Against Prostate Cancer Through Inducing Apoptosis. Technol. Cancer Res. Treat. *20*, 1533033821995284. https://doi.org/10.1177/1533033821995284.

120. Shinada, H., Watanabe, T., Okudaira, K., Iwase, Y., Nishi, K., and Yumita, N. (2019). Apoptosis Induced by Ultraviolet A Exposure in the Presence of Enoxacin in HL-60 Cells. Anticancer Res. *39*, 687–693. https://doi.org/10.21873/anticanres.13164.

121. Nishi, K., Kato, M., Sakurai, S., Matsumoto, A., Iwase, Y., and Yumita, N. (2017). Enoxacin with UVA Irradiation Induces Apoptosis in the AsPC1 Human Pancreatic Cancer Cell Line Through ROS Generation. Anticancer Res. *37*, 6211–6214. https://doi.org/10.21873/anticanres.12071.

Please cite this article in press as: Lee et al., Host-transposon mutualism supports regeneration in planarians, Developmental Cell (2026), https://doi.org/10.1016/j.devcel.2026.03.001

STAR★METHODS

KEY RESOURCES TABLE

REAGENT or RESOURCE	SOURCE	IDENTIFIER
Antibodies		
Rabbit polyclonal B-IAP	This paper	N/A
Mouse monoclonal anti-FLAG	Sigma-Aldrich	Cat#F1804; RRID: AB_262044
Rabbit polyclonal anti-HA	Abcam	Cat#ab9110; RRID: 307019
Rabbit polyclonal anti-caspase-3	Abcam	Cat#ab13847; RRID: 443014
Mouse anti-α-tubulin	Millipore	Cat#MABT205; RRID: AB_11204167
Mouse anti-actin	Millipore	Cat#MABT825; RRID: AB_2571580
Mouse monoclonal anti-Rabbit IgG, HRP	Cell Signaling Technology	Cat#5127S; RRID: AB_10892860
Rat monoclonal anti-mouse IgG, HRP	Abcam	Cat#ab131368; RRID: AB_2895114
Mouse Normal IgG	Cell Signaling Technology	Cat#5415S; RRID: AB_10829607
Goat polyclonal anti-Rabbit IgG, HRP	Abcam	Cat#ab6721; RRID: AB_955447
Goat polyclonal anti-Mouse IgG, HRP	Abcam	Cat#ab6789; RRID: AB_955439
Sheep polyclonal anti-DIG-POD	Roche	Cat#11207733910; RRID: AB_514500
Sheep polyclonal anti-Fl-POD	Roche	Cat#11426346910; RRID: AB_840257
Rat monoclonal anti-DNP-HRP	Perkin Elmer	Cat#FP1129; RRID: AB_2629439
Bacterial and virus strains		
DH10B F- mcrA Δ(mrr-hsdRMS-mcrBC) Φ80dlacZΔM15 ΔlacX74 endA1 recA1 deoR Δ(ara,leu)7697 araD139 galU galK nupG rpsL λ–	New England Biolabs	Cat#C3019I
BL12 (DE3) fhuA2 [lon] ompT gal (λ DE3) [dcm] ΔhsdSλ DE3 = λ sBamHIo ΔEcoRI-B int::(lacI::PlacUV5::T7 gene1) i21 Δnin5	New England Biolabs	Cat#C2530H
Chemicals, peptides, and recombinant proteins		
Actinomycin-D (Act-D)	Sigma-Aldrich	Cat#A1410
Ampure XP beads	Beckman Coulter	Cat#A63881
Anti-FLAG® M2 Magnetic Beads	Sigma-Aldrich	Cat#M8823
Benzamidine Separopore 6B	bioWORLD	Cat#20181111-2
c0mplete Mini, EDTA-free	Roche	Cat#11836170001
cyclohexamide	Sigma-Aldrich	Cat#1810
Digoxigenin-11-dUTP	Roche	Cat#11093088910
DMEM, high glucose, pyruvate	GIBCO	Cat#11995065
DMSO	New England Biolabs	Cat#B0515A
DNaseI	New England Biolabs	Cat#M0303S
DPBS	GIBCO	Cat#14190-144
DTT	ThermoFisher	Cat#BP17225
Enoxacin	ThermoFisher	Cat#J61912.06
EvaGreen	New England Biolabs	Cat#1725213
Fetal bovine serum	Sigma-Aldrich	Cat#F0926
Formaldehyde	ThermoFisher	Cat#119690010
Formamide (deionized)	Ambion	Cat#AM9344
Gentamicin Sulfate Salt	Sigma-Aldrich	Cat#G1264-1G
glutathione-sepharose beads	ThermoFisher	Cat#16101
Hydrogen Peroxide	Sigma-Aldrich	Cat#7722-44-1
L-glutamine	GIBCO	Cat#25030-081

(*Continued on next page*)

Please cite this article in press as: Lee et al., Host-transposon mutualism supports regeneration in planarians, Developmental Cell (2026), https://doi.org/10.1016/j.devcel.2026.03.001

Continued

REAGENT or RESOURCE	SOURCE	IDENTIFIER
LongAmp Taq 2XMaster Mix	New England Biolabs	Cat#M0287
Maxima H Minus Reverse Transcriptase	ThermoFisher	Cat#EP0752
2-Mercaptoethanol	Sigma-Aldrich	Cat#M3148
Pen-strep	GIBCO	Cat#15140-122
PMSF	MP Biomedicals	Cat#219538105
Polyethylenimine (PEI)	Kyfora Bio	Cat#23966-100
Proteinase K	Invitrogen	Cat#25530049
Protoscript II RT	New England Biolabs	Cat#M0368L
RNaseH	New England Biolabs	Cat#M0297L
ScaI-HF	New England Biolabs	Cat#R3122S
Terminal Transferase	New England Biolabs	Cat#M0315S
Triton X-100	Sigma-Aldrich	Cat#SLBW6852
Trizol	Life Technologies (ambion)	Cat#15596018
Trypsin-EDTA	Invitrogen	Cat#25300-054
Tween-20	Sigma-Aldrich	Cat#P7949
Critical commercial assays		
Ac-YVAD-AFC	Cayman	Cat#17591
Ac-IETD-AFC	Cayman	Cat#17480
Ac-LEHD-AFC	Cayman	Cat#17051
Caspase 3 Detection Kit	Abcam	Cat#ab102491
cDNA-PCR sequencing Kit	Oxford Nanopore	Cat#SQK-PCS109
Monarch® Plasmid Miniprep Kit	New England Biolabs	Cat#T1110L
Nucleospin Gel and PCR Clean-up kit	Machery-Nagel	Cat#740609
Deposited data		
Regeneration data re-processed (Figures S2I and S3E)	Wurtzel et al.[57]	PRJNA276084
Planarian transcriptomic data re-processed (discussion)	Vila-Farre et al.[83]	PRJNA1011852
Nanopore sequencing data	This paper	PRJNA1135975
Schmidtea mediterranea genome	Ivankovic et al.[89]	Planmine[90]
Dugesia japonica genome	An et al.[91]	http://www.planarian.jp
Genome and Transcriptomes	This paper	see Table S2
Western blots	This paper	Mendeley: 10.17632/8gk5ssdtvp.1
Experimental models: Cell lines		
Human: HEK293T	ATCC	CRL-3216
Experimental models: Organisms/strains		
S. mediterranea: asexual CIW4 clonal line	Lab stock	N/A
Oligonucleotides		
primers	This paper	see Table S1
Recombinant DNA		
pGEM-T	Promega	Cat#A3600
pCDNA 3.1	ThermoFisher	Cat#V790-20
pCMV3flag8HOIL-1L	Fu et al.[92]	Addgene Cat#50016
pGEX-XIAP	Yang et al.[93]	Addgene Cat#8340
pGEM-Gypsy8	This Paper	N/A
pGEM-BURRO2	This Paper	N/A
pGEM-B1-5'MATH	This Paper	N/A
pGEM-SLF9	This Paper	N/A
pGEM-BURRO1-IAP	This Paper	N/A

(*Continued on next page*)

Please cite this article in press as: Lee et al., Host-transposon mutualism supports regeneration in planarians, Developmental Cell (2026), https://doi.org/10.1016/j.devcel.2026.03.001

Continued

REAGENT or RESOURCE	SOURCE	IDENTIFIER
pGEX-BIAP-GST	This Paper	N/A
pcDNA-IAP2-3xflag	This Paper	N/A
pcDNA-B-IAP-3xflag	This Paper	N/A
pcDNA-Caspase9038-3xflag	This Paper	N/A
pcDNA-BIAP	This Paper	N/A
pcDNA-Caspase9038-3xHA	This Paper	N/A
pcDNA-Caspase10708-3xHA	This Paper	N/A
pcDNA-Caspase11193-3xHA	This Paper	N/A
Software and algorithms		
RepeatMasker (v4.1.2-p1-foss-2020b)	Smit et al.[94]	https://www.repeatmasker.org/
MAFFT v7	Katoh et al.[95]	https://mafft.cbrc.jp/alignment/software/source.html
MEGA11	Tamura et al.[96]	https://www.megasoftware.net
SeqKit (v2.8.1)	Shen et al.[97]	https://bioinf.shenwei.me/seqkit/
EMBOSS Needle	Rice et al.[98]	https://www.ebi.ac.uk/jdispatcher/psa/emboss_needle
BLAST+ version 2.15.0	Camacho et al.[99]	https://blast.ncbi.nlm.nih.gov/doc/blast-help/downloadblastdata.html#downloadblastdata
RAxML-NG v1.2.1	Kozlov et al.[100]	https://github.com/amkozlov/raxml-ng
MRBAYES version 3.2.7	Ronquist et al.[101]	https://nbisweden.github.io/MrBayes/download.html
interactive Tree of Life (iTOL)	Letunic et al.[102]	https://itol.embl.de/
VISTA	Frazer et al.[103]	https://genome.lbl.gov/vista/mvista/submit.shtml
fastp (version 0.21.0)	Chen et al.[104]	https://github.com/OpenGene/fastp
STAR (version 2.7.2a)	Dobin et al.[105]	https://github.com/alexdobin/STAR
FeatureCounts (version 1.6.4)	Liao et al.[106]	https://subread.sourceforge.net/
R Project for Statistical Computing v4.10	The R Foundation	https://www.r-project.org/
GraphPad Prism	GraphPad Software	https://www.graphpad.com/scientific-software/prism/
Planarian Image Quantification (PIQ) package v1.0.5	Allikka Parambil et al.[55]	https://gitlab.com/vanwolfswinkel/PIQ
Alphafold2	Jumper et al.[107]; Liu et al.[108]; Mirdita et al.[109]	https://colab.research.google.com/github/sokrypton/ColabFold/blob/main/AlphaFold2.ipynb
ImageJ (FIJI)	Schindelin et al.[110]	https://fiji.sc

EXPERIMENTAL MODEL AND STUDY PARTICIPANT DETAILS

Planarian strain and husbandry

Schmidtea mediterranea asexual clonal strain ClW4 was maintained as previously described.[111] Briefly, animals were cultured in 1x Montjuic salts at 20°C, fed homogenized beef liver paste every 1–2 weeks, and expanded through continuous cycles of amputation or fissioning and regeneration. Animals were starved 1-2 weeks prior to experiments, and assigned to control or treatment by randomized selection. For RNAi experiments, water was supplemented with 50ug/ml Gentamicin sulfate (VWR) to prevent bacterial growth.

Cell culture

Human embryonic kidney 293 (HEK293) cells were maintained in Dulbecco's Modified Eagle Medium (DMEM; high glucose) with 10% fetal bovine serum and 1% penicillin-streptomycin. Cultures were incubated at 37°C in a humidified atmosphere containing 5% CO_2. Cells were routinely passaged at ~80% confluence using trypsin-EDTA.

HEK293 cells were originally derived from the kidney of a female human embryo. Cells were obtained directly from ATCC where authentication is conducted prior to distribution.

Please cite this article in press as: Lee et al., Host-transposon mutualism supports regeneration in planarians, Developmental Cell (2026), https://doi.org/10.1016/j.devcel.2026.03.001

METHOD DETAILS

RNAi and drug treatment

Regions of planarian genes 0.5-2kb in length were amplified from complementary DNA (cDNA) using sequence specific primers (Table S1). The PCR product was cloned into the pGEM-T vector (Promega) and verified by Sanger sequencing. Both RNA strands were synthesized *in vitro* from PCR-generated forward and reverse templates with flanking T7 promoters (TAATACGACTCACTA TAGG), and annealed by incubation at 37°C for 30min. The transcribed ssRNAs as well as the final hybridized dsRNA product were verified by gel electrophoresis.

Size-matched animals were starved 1-2 weeks prior to experiments and assigned to treatment conditions by random selection. Experiments were performed on batches of 6-12 animals, and were repeated at least 3 times. No technical replicates are used.

RNAi food was prepared by combining 2ul dsRNA with 2ul food coloring and 50ul of homogenized beef liver.[112] *Burro1(RNAi)* animals were fed dsRNA on day 0, and subsequently injected with dsRNA (without additions) three more times (on day 2, day 7 and day 9). DsRNA matching *C. elegans* gene *unc-22* was used as a negative control. Efficiency of RNAi was verified by qPCR prior to further experiments, and if necessary, animals with ineffective RNAi were removed.

The RNAi constructs used in this study targeted the *B-iap* part of the Burro1 transposon. However, as Burro1 is likely mainly transcribed as one long transcript that originates from the 5'LTR, targeting of *B-iap* results in simultaneous reduction of the rest of the Burro1 transcript.

For inhibition of transcription, 2ul of Actinomycin D (5mg/ml in DMSO) was combined with 2ul food coloring and 35ul of homogenized beef liver. Animals were processed for amputation at 16 hours after feeding. DMSO was used instead of Actinomycin as a control treatment.

Stress conditions

Amputations were performed posterior to the pharynx by razor blade incision.

For irradiation, animals were placed in 6cm dishes with 6ml of water and exposed to the indicated dose of gamma irradiation after Thoreaux filter in a MultiRad350 (Precision Inc) in exposure control mode. Animals were subsequently maintained in water supplemented with 50ug/ml Gentamicin sulfate (VWR).

For drought exposure, animals were transferred to a clean 6 cm dish. Water was removed carefully, avoiding the collection of animals at the edges of the plate. Animals were left without water for 20 minutes, after which water was replenished.

For heat stress, animals were moved to a clean plate and water was replaced by planarian water preheated to 30°C. Plates were incubated in an oven at 30°C for 10 min. After the incubation was complete, water was removed and replaced by room temperature water three times to rapidly bring the temperature down.

Whole-mount fluorescent in situ hybridization and immunofluorescence

Fixations and whole-mount *in situ* hybridizations (ISH) and immunofluorescence were performed as previously described,[113] with alterations described in King and Newmark[114]. Briefly, formaldehyde fixed animals were bleached using formamide bleach solution and treated with proteinase K (2 ug/ml) in PBSTx (PBS containing 0.1% Triton X-100). For FISH, following overnight hybridization at 56°C, samples were washed sequentially in pre-hyb solution, 1:1 pre-hyb-2x SSC, 2x SSC and 0.2x SSC at 56°C. Probes were detected with anti-DIG-POD (Roche 11207733910), anti-Fl-POD (Roche 11426346910), or anti-DNP-HRP (Perkin Elmer PF1129). After tyramide development,[114] peroxidase was inactivated by incubation in 1% sodium azide for 1.5 hour if additional tyramides were used. Specimens were counterstained with DAPI (Sigma). For immunofluorescence of phosphorylated histone 3, animals were blocked and incubated with primary antibody anti-phospho-Histone3[Ser10] (Millipore, clone 63-1C-8) 1:750 overnight, followed by incubation with goat anti-Mouse IgG HRP Conjugate (Life Technologies). Signals were developed using Tyramide SuperBoost™ Kits (Invitrogen).

For TUNEL staining, after fixation and bleaching, animals were incubated in TUNEL reaction buffer (25mM Tris-HCl, 200 mM Sodium Cacodylate, 0.25 mg/ml BSA, 1mM Cobalt Chloride) for 30 min before addition of 8U of TdT enzyme (NEB) and 120pmol DIG-dUTP (Roche). Reactions were incubated for 1 hour at 37°C in a humid chamber, followed by washes in PBSTx and detection using anti-DIG-POD and tyramide amplification as described above.

Neoblast isolation and staining

Neoblasts in G2/M phase (X1) and differentiated cells (Xins) were isolated by Fluorescence-Activated Cell Sorting based on DNA content as determined by Hoechst intensity,[115] following standard procedures described previously.[116]

For staining of the isolated cells, FACS-sorted cells were washed in CMF, spotted onto poly-D-lysine coated coverslips (BD Biosciences) positioned in 24 well plates, allowed to settle for 30 minutes, and fixed in 4% PFA (in PBS) for 20 minutes at room temperature. Controls and treatment were always spotted on the same cover slip, and went through all staining steps in the same well. FISH labelings were carried out similarly to the whole-mount protocol, with wash steps and antibody incubations shortened to 10 minutes and 1 hour, respectively.

Please cite this article in press as: Lee et al., Host-transposon mutualism supports regeneration in planarians, Developmental Cell (2026), https://doi.org/10.1016/j.devcel.2026.03.001

Microscopy and image analysis

Images were acquired on a Zeiss LSM800 Confocal Microscope. Control and RNAi animals were imaged with the same magnification, laser intensity and gain, at comparable anatomical position. Images were generated in Image J.[110] Cell counting and quantification of fluorescence intensity were performed using the automated quantification scripts in the Planarian Image Quantification (PIQ) package v1.0.5.[55]

qPCR analysis

Total RNA was isolated by Trizol and quantified by Qubit. RNA was treated with DNaseI (Promega) for 30 minutes at 37°C and cleaned by precipitation on Ampure beads. cDNA was synthesized using oligo dT primers and ProtoScriptII (NEB) according to the manufacturer instructions. qPCR reactions were performed using EvaGreen mastermix (Biotium). Primers are listed in Table S1. RT and qPCR reactions of samples and controls were run in parallel in the same plates. qPCRs were run on a QuantStudio 3 instrument (ABI) with the following program: 95°C, 20s; 40 cycles of 95°C, 5s; 60°C, 20s; followed by a melting curve analysis.

For the quantification of transposon copy numbers by genomic qPCR, five regions corresponding to four transposable elements—Slf9, Gy8, B2, B1 5'Math, and B1 IAP—were PCR-amplified from cDNA using sequence-specific primers (Table S1), and cloned into the pGEM-T vector (Promega). Positive clones were verified by Sanger sequencing. Plasmids (1 μg) were linearized with ScaI (NEB) at 37°C for 1 h, followed by enzyme inactivation at 80°C for 20 min. The number of molecules was calculated for each preparation, based on plasmid size and DNA concentration. Serial dilutions of each plasmid were prepared to generate standard curves with final copy numbers of 1×10^7, 1×10^6, 1×10^5, 1×10^4, and 1×10^3 molecules/μL.

Genomic DNA was extracted from sexual and asexual Schmidtea mediterranea using the CTAB method.[41] Residual RNA was removed by treatment with 1 μL RNase A (NEB) at 37°C for 30 min. DNA was further purified using NucleoSpin Gel and PCR Clean-up kit (Macherey-Nagel) per the manufacturer's protocol. DNA quality and concentration were assessed using a Nanodrop spectrophotometer (DeNovix). Extracted genomic DNA from planarians was normalized to 0.1 ng/μL and used as a template for qPCR. Reactions were performed using a EvaGreen master mix (Biotium) with primers specific to each transposon target region (Table S1). Standard curves were run in parallel to genomic DNA samples, and the resulting Ct values were used to interpolate the absolute copy numbers of each transposon in genomic DNA samples.

To estimate the genomic copy number of each transposon, qPCR amplicon sequences were queried against the *S. mediterranea* reference genome (smed_chr_ref_v1.fa; Guo et al.[117]) using NCBI BLAST+ (default parameters). The number of BLAST hits corresponding to high-identity matches was counted as the bioinformatically predicted genomic copy number. To compare experimental copy numbers obtained by qPCR with BLAST-based predictions, values were normalized to the copy number of Slf9, which served as an internal reference due to its recent insertion and presumed low sequence divergence. Relative abundance for each transposon was calculated by dividing both qPCR-derived and BLAST-derived copy numbers by that of Slf9.

Polysome profiling

Polysome profiling was carried out as described in Allikka Parambil et al.[55] and Panda et al.[118] Briefly, worms were treated with cycloheximide (100 μg/ml) for 48 hours and lysates were prepared by flash-freezing the worms in liquid nitrogen using pre-chilled polysome extraction buffer (20 mM Tris-HCl pH 7.5, 150 mM NaCl, 1.5 mM $MgCl_2$, 0.6% Triton X-100, 0.5 mM DTT, 1× protease inhibitor, and 100 μg/ml cycloheximide), followed by mechanical grinding and douncing. The lysates were cleared by centrifugation (12000 g for 10 min at 4°C). Cleared lysate was layered on the top of a 10–50% sucrose density gradient prepared in the buffer and subjected to ultracentrifugation at 40000 RPM for 16 h at 4°C (Beckman SW 41 Ti rotor). Fractions were collected by upward displacement and the absorbance was monitored at 254 nm to localize the monosome and polysome peaks. Monosome- and polysome-containing fractions were pooled, and RNA was purified by TRIzol extraction for cDNA synthesis.

Nanopore sequencing and 5'RACE

Nanopore sequencing libraries were prepared using the cDNA-PCR Sequencing Kit (SQK-PCS109, ONT) according to the manufacturer's instructions. Additional RACE libraries were generated by reverse transcription and template-switching by Maxima H Minus Reverse Transcriptase (Thermo Fisher Scientific Inc.), using six reverse primers specific to Burro1 and a common adapter. Nanopore amplicons were generated from cDNA with LongAmp Taq master mix (New England Biolabs, USA) and the Nanopore cDNA sequencing kit according to the manufacturer's instructions. PCR products were purified using the AMPure XP beads (Beckman Coulter, USA). Sequencing was performed on a MinION Mk1B system (Oxford Nanopore Technologies Ltd., ONT), using a FLO-MIN106 flow cell. Basecalling was performed using guppy (ONT guppy v4.4.1., github.com/nanoporetech/rerio). Adapters were trimmed using Porechop (github.com/rrwick/Porechop). Only reads with a minimum Q score of 10 were selected for analysis of *Burro1* transcripts.

In vitro caspase assays

B-IAP was cloned before a FLAG tag in the pcDNA 3.1 vector and expressed in HEK293T cells by polyethyleneimine (PEI)-mediated transfection. Empty vector transfected into HEK293T was used as a negative control. HEK293T cells were lysed by pipetting in pre-chilled lysis buffer (20mM Tris-HCl pH7.5, 150mM NaCl, 1.5mM MgCl2, 0.6% Triton X-100, 0.5mM DTT, 1X protease inhibitor, 1 mM PMSF) and lysates were cleared by centrifugation at 5,000 × g for 5 min at 4°C.

Please cite this article in press as: Lee et al., Host-transposon mutualism supports regeneration in planarians, Developmental Cell (2026), https://doi.org/10.1016/j.devcel.2026.03.001

Apoptosis was induced by incubating live animals in 1mM enoxacin water for 24 hours followed by exposure to 550mJ/cm2 of UV irradiation in a UV crosslinker (UVP).[119–121] Two hours after UV exposure lysates were prepared by grinding the animals in pre-chilled lysis buffer (20mM Tris-HCl pH7.5, 150mM NaCl, 1.5mM MgCl2, 0.6% Triton X-100, 0.5mM DTT, 1X protease inhibitor, 1 mM PMSF). Lysates were subsequently cleared by centrifugation at 5,000 × g for 5 min at 4°C. Cleared planarian lysates were supplemented with a fluorescent substrate and HEK293T cell lysate (control, or containing B-IAP protein) and incubated for one hour at 37°C to measure caspase activity. We had determined that planarian initiator caspases cleave the VLAD motif, however as this motif is not favored by any mammalian caspase, no commercial Ac-VLAD-AFC was available. We thus tested several substrates for motifs with similar animo acid characteristics, namely Ac-YVAD-AFC (Cayman 17591), Ac-IETD-AFC (Cayman 17480), and Ac-LEHD-AFC (Cayman 17051), and Abcam Caspase 3 Detection Kit (ab102491) containing Ac-DEVD-AFC. Caspase activity was quantified using a plate reader (Bio-Tek; ex 400 nm / em 505 nm).

Protein structure predictions

Predictions of protein structure were performed using Alphafold2 in ColabFold.[107,108,109] BIR domains of the three planarian IAP proteins (IAP-1 residues 54-156, IAP-2 residues 83-185, BURRO1 IAP residues 62-164) and the eight planarians caspases (dd_Smed_v4_10708 residues 169-427, dd_Smed_v4_9038 residues 172-427, dd_Smed_v4_11193 residues 116-391, dd_Smed_v4_10883 residues 239-497, dd_Smed_v4_3121 residues 1-266, dd_Smed_v4_4986 residues 1-263, dd_Smed_v4_8326 residues 1-248, dd_Smed_v6_1167 residues 1-252) were used to predict interactions between the IAP proteins and the caspases. To compute the complex structure of the BIR domain with the caspase we used three cycles and 5 models, using the "multimer-2" option.

Predictions were rerun with Alphafold3 with similar outcomes.

In vitro interaction assays

HEK293 cells were maintained in Dulbecco's modified Eagle's medium (DMEM; Gibco) supplemented with 10% (v/v) fetal bovine serum (FBS; Gibco) and 1× penicillin–streptomycin (Gibco). Cells were seeded in 15 cm dishes to ~70% confluence and transiently transfected with a plasmid encoding C-terminally FLAG-tagged planarian B-IAP, C-terminally FLAG-tagged Genomic IAP-2, and C-terminally HA-tagged Caspase, using Polyethylenimine, Linear, MW 25000, Transfection Grade (PEI 25K™) according to the manufacturer's instructions. 48 hrs post-transfection, cells were washed twice with cold PBS and lysed in ice-cold lysis buffer (50 mM Tris-HCl pH 7.5, 150 mM NaCl, 1 mM EDTA, 1% Triton X-100, and 1× protease inhibitor cocktail (Roche)) for 5,000 × g for 5 min at 4°C, and the supernatants were incubated with either anti-FLAG (M2) magnetic agarose resin (Millipore Sigma) or protein G magnetic beads (NEB) for 2 hr 4°C with gentle rotation. Resin was washed three times with wash buffer (50 mM Tris-HCl pH 7.5, 150 mM NaCl, 0.1% Triton X-100), and bound protein was eluted with acid-glycine buffer. The eluates were denatured in protein loading buffer (60mM Tris-Cl pH6.8, 5% Glycerol, 1% SDS and 2.5% β-mercaptoethanol) and used for immunoblotting as described below.

To test the binding of native B-IAP protein to planarian caspase, C-terminally FLAG-tagged Caspase-9038 protein was generated in HEK293T cells as described above. HEK293T cell lysate was combined with planarian lysate generated in the same buffer and incubated with anti-FLAG (M2) magnetic agarose resin (Millipore Sigma) for 2 hours at 4°C. Resin was washed in wash buffer and bound protein was eluted with acid-glycine buffer. The eluates were denatured in protein loading buffer and used for immunoblotting as described below.

While both the computational predications and the *in vitro* experiments supported the interaction of the B-IAP protein with initiator caspases, the two methods produced slightly different outcomes. The computational modeling predicted an interaction of B-IAP with Caspase_10708. The in vitro experiment confirmed this interaction, but found a stronger interaction with Caspase_9038. Further, whereas the modeling had indicated that B-IAP was a better binder of caspases, *in vitro* experiments found that the genomic IAP-2 protein was similar in its binding efficiency. The reason for these discrepancies probably lies in two major limitations in the modelling. In the first place, the modelling used only the BIR domain of B-IAP, as modeling of the full IAP protein did not result in a reliable structure. The IP however used the full B-IAP protein. In the second place, caspases are typically cleaved into a small and large subunit preceded by a less structured N-terminal region. The modeling used the caspase without this N-terminal sequence because this region disrupted the predicted caspase structures. This region again was present in the *in vitro* experiments.

B-IAP antibody generation

GST-tagged B-IAP was cloned into pGEX. The recombinant protein constructs were overexpressed in BL21(DE3) by induction with 0.2 mM isopropyl thio-β-D-galactoside (IPTG) at 15°C and purified using pre-equilibrated glutathione-sepharose beads (Invitrogen) as described previously.[55] Buffers were supplemented with protease inhibitor cocktail (Roche), DNase I and RNase A to rule out interactions through nucleic acids. All the procedures were carried out at 4°C. Proteins were concentrated with membrane filters, snap frozen and stored in -80°C.

Immunizations of rabbit hosts were performed by Cocalico Biologicals, Inc. B-IAP antibodies were purified from rabbit serum by affinity purification using B-IAP protein coupled to CNBr-activated Sepharose (Cytiva). Purified antibodies were snap frozen and stored in -80°C.

SDS-PAGE and Western blotting

Individual 1-3mm sized animals were homogenized in protein loading buffer (60mM Tris-Cl pH6.8, 5% Glycerol, 1% SDS and 2.5% β-mercaptoethanol) and separated on 8% denaturing polyacrylamide gel. Samples were transferred to PVDF membrane, blocked in

PBST (PBS with 0.1% Tween-20) with 3% milk powder, and incubated with the primary antibody followed by secondary antibody, in PBST with 1.5% milk powder. The following commercial antibodies were used: mouse anti-α-tubulin (Millipore) at 1:10000; caspase-3 (Abcam) 1:500; mouse anti-FLAG M2 antibody (1:5000); mouse Normal IgG (Cell Signaling Technologies); goat anti-Rabbit IgG HRP Conjugate at 1:10000 and goat anti-Mouse IgG HRP Conjugate (Life Technologies) at 1:10000. Additionally, B-IAP antibody (described above) at 1:1000, and antibodies labeling PIWI proteins SMEDWI-1and SMEDWI-2[55,54] at 1:1000 and 1:2000 respectively were used.

Phylogenetic analysis

Genome and transcriptome sequences were retrieved from publicly available databases including giri REPBASE (https://www.girinst.org/repbase/), planarian.jp (http://www.planarian.jp), WormBase Parasite (https://parasite.wormbase.org/ftp.html), NCBI GenBank (https://www.ncbi.nlm.nih.gov), SMART (https://smart.embl.de/domains.cgi), Zenodo (https://doi.org/10.5281/zenodo.8301321), and PlanMine (https://planmine.mpinat.mpg.de/planmine/begin.do). Accession numbers and dataset versions are detailed in Table S2.

For the analysis of the transposon copies, consensus transposon sequences as listed on Repbase (https://www.girinst.org/repbase/) were used to identify individual copies in the *S. mediterranea* genome using RepeatMasker (v4.1.2-p1-foss-2020b).[94]

For analysis of sequence variation in the I-region (sequence without the LTRs) of the Ty3 transposable elements (TE), genomic sequences corresponding to 90–110% of the I-region length—based on the Ty3 reference TE—were extracted from Ty3 elements mapped to the *S. mediterranea* genome and exported in FASTA format. TE sequences were grouped by subfamily and aligned separately using MAFFT v7.[95] Pairwise evolutionary distances (p-distance) were calculated for each TE using MEGA11.[96]

For analysis of the LTR divergence, only SLF, gy14, B1, and B2 TEs with both 5′ and 3′ long terminal repeats (LTRs) were retained for further analysis. The flanking 5′ and 3′ LTR sequences for each TE were extracted from the genome using SeqKit (v2.8.1)[97] and exported in FASTA format. Pairwise global alignment between the 5′ and 3′ LTR sequences of each TE was performed using EMBOSS Needle[98] to calculate percentage similarity.

Domain-containing sequences (IAP, LTR, MATH, and Ty3 pol) were identified using BLAST+ version 2.15.0[99] on the Yale McCleary HPC cluster. Searches used blastn against genome and transcriptome assemblies with the -task blastn parameter and an E-value threshold of 1e-5. Query sequences were provided in unmasked FASTA format. Nucleotide sequences for each genic element were aligned using MAFFT version 7.[95] Maximum likelihood (ML) analyses were performed with RAxML-NG v1.2.1[100] applying the GTR+G model of nucleotide substitution, with node support assessed by 20,000 bootstrap replicates. Bayesian phylogenetic inference was performed separately for each gene alignment using MRBAYES version 3.2.7.[101] Two independent Markov chain Monte Carlo (MCMC) runs, each with four incrementally heated chains, were run for 10 million generations, sampling every 5,000 generations. The initial 25% of samples were discarded as burn-in, and convergence was confirmed by standard diagnostics. Consensus trees were constructed from post-burn-in samples. Phylogenetic trees were visualized and annotated with the Interactive Tree of Life (iTOL) online tool.[102] Bootstrap and posterior probability support values were combined and annotated on the ML consensus tree using Adobe Illustrator.

Protein sequences of Caspases and BIR-domain proteins were aligned using MAFFT v7.[95] Maximum likelihood analyses were conducted using RAxML-NG v1.2.1[100] with the LG+G8+F substitution model. The analysis was run using the –all option on the MAFFT-aligned dataset, with 2,000 bootstrap replicates (–bs-trees 2000), a bootstrap support cutoff of 0.01 (–bs-cutoff 0.01), and both FBP and TBE bootstrap metrics enabled (–bs-metric fbp,tbe). Analyses were performed using automatic thread allocation (–threads auto). Resulting ML trees were visualized using standard tree-viewing software (iTOL).

For the analysis of synonymous and non-synonymous mutations, the genome sequence of *Dugesia japonica* was obtained from Planarian.jp (http://www.planarian.jp),[91] and the transcriptome data were retrieved from PlanMine (https://planmine.mpinat.mpg.de). The *Schmidtea mediterranea* BURRO1_I sequence was used as a query for BLAST searches to identify the homologous BURRO1 sequence in *D. japonica*. Conserved regions between species were visualized using global alignments and VISTA.[103] Synonymous (dS) and nonsynonymous (dN) substitution rates were calculated using MEGA11.[96]

Processing of mRNA-seq data

Publicly available mRNA libraries (PRJNA276084) were reanalyzed by mapping against the *Schmidtea mediterranea* genome.[89] Reads were filtered and trimmed using fastp (version 0.21.0)[104] with parameters –length_required 20 –average_qual 20. Mapping was performed using STAR (version 2.7.2a)[105] with the following settings: –outFilterMismatchNmax 2 –alignIntronMax 15000 –alignMatesGapMax 15000 –outFilterMultimapNmax 100 –winAnchorMultimapNmax 100. FeatureCounts (version 1.6.4)[106] was used to count the reads/fragments over the gene annotations with parameters -M -C -O. Heatmaps were generated using pheatmap on R v4.10.

QUANTIFICATION AND STATISTICAL ANALYSIS

All reported measurements were made from distinct samples. Levels of significance were calculated by two-tailed Student's t test, using the Prism software package. Error bars indicate standard deviations. Whiskers on box plots indicate min and max observations.

Developmental Cell, Volume *61*

Supplemental information

Host-transposon mutualism supports regeneration in planarians

Hae-Lim Lee, Axel Poulet, Sudheesh Allikka Parambil, and Josien C. van Wolfswinkel

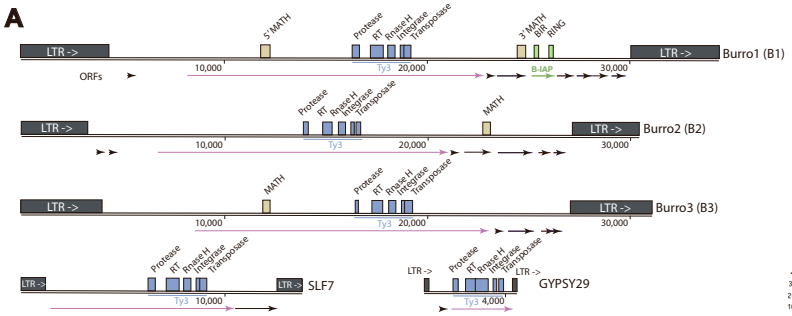

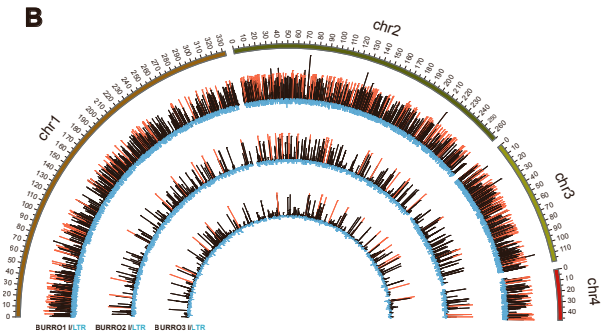

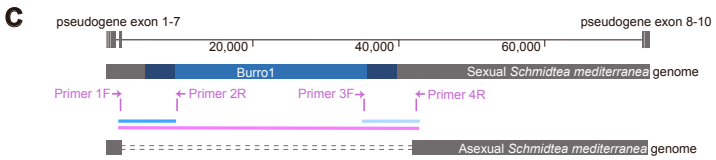

	sample	primers	expected size
1	Asexual	Primer 1F/Primer 4R	881 bp
2	Sexual	Primer 1F/Primer 4R	40,279 bp
3	Asexual	Primer 1F/Primer 2R	x
4	Sexual	Primer 1F/Primer 2R	7,790 bp
5	Asexual	Primer 3F/Primer 4R	x
6	Sexual	Primer 3F/Primer 4R	7,048 bp

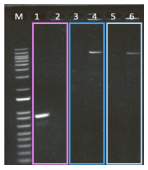

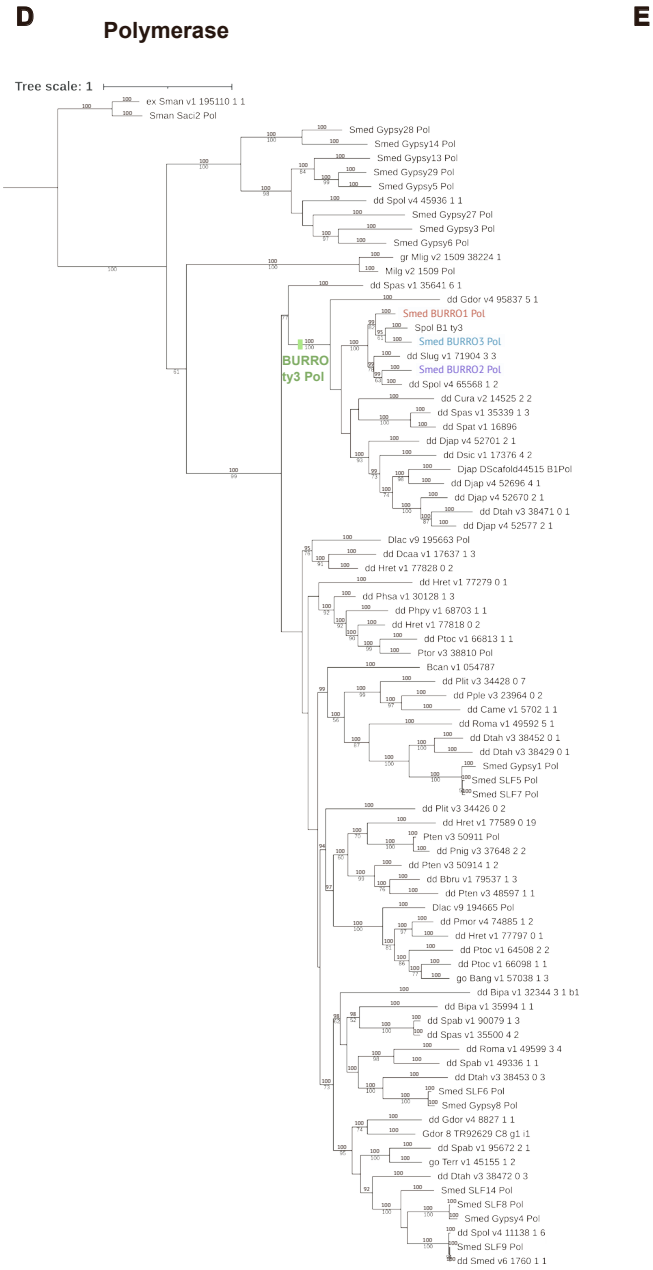

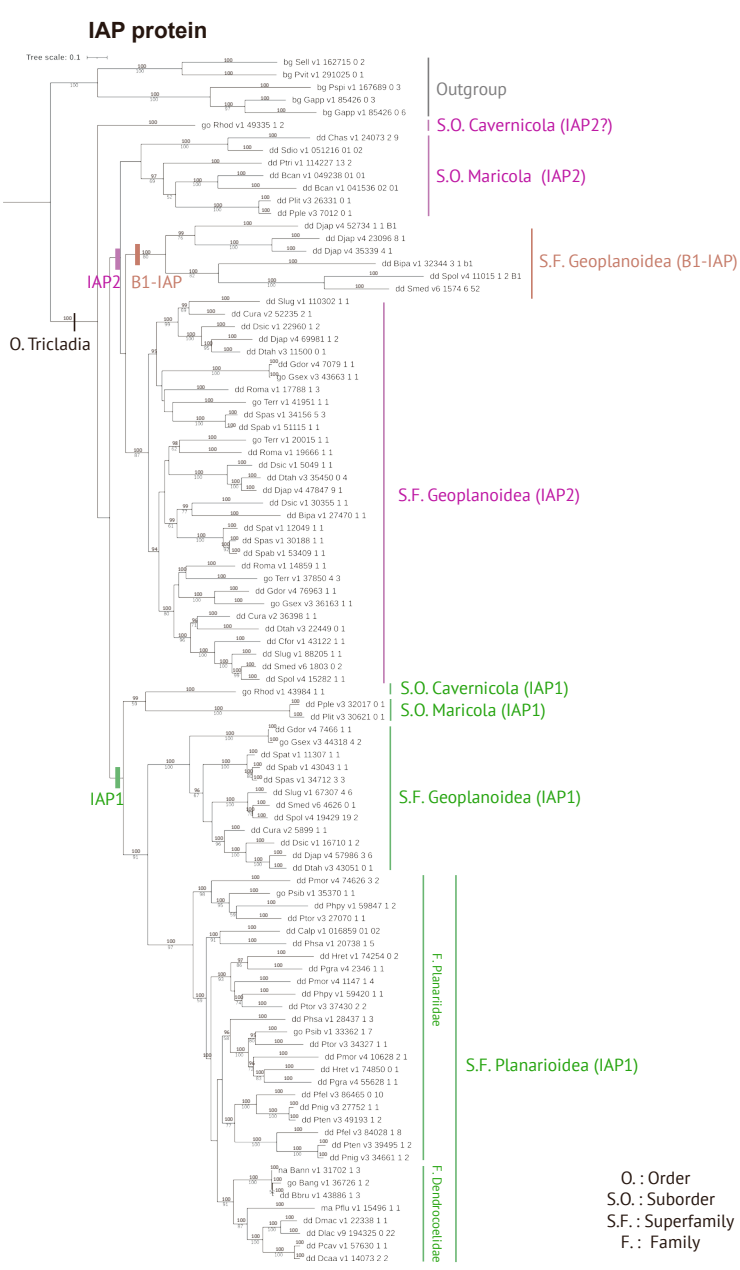

O. : Order
S.O. : Suborder
S.F. : Superfamily
F. : Family

Figure S1. Life history of Burro1. Related to Figure 1.

(A) Schematic showing the domains encoded in the three Burro elements. Two "normal-sized" Ty3 elements are shown for comparison. Burro elements have unique characteristics, which revealed that they are present only in a small group of flatworms. They could have entered this clade of flatworms by horizontal transfer from another species, or by recombination of elements within the flatworm genome that resulted in a more successful mobile element. We investigated the various components that make up the Burro element to determine whether they appear to be novelties that likely came from an exogenous origin, or whether they show resemblance to elements that are present elsewhere in the planarian genome in which case they could have arisen by recombination.

(B) Length and genomic distribution of the Burro elements over the four chromosomes of the *S. mediterranea* genome. Full length copies are indicated in red. Full length elements are not all closely related, indicating that multiple independent copies are still active in the genome.

(C) PCR dat (right) and primer organization (left) showing a novel Burro1 insertion in the sexual strain of *S. mediterranea*, that is absent from the asexual strain, located in a pseudogene. This indicates that Burro1 has recently generated new insertions in the planarian genome.

(D) Phylogenetic tree of the Polymerase sequence of the Burro elements relative to other planarian Ty3 elements. The core retrotransposon genes of the 3 Burro transposons are closely related to each other, and to other Ty3 elements. Ty3 elements are widespread through plants and animals. Out of all Ty3 elements we investigated, the Burro Ty3 polymerases however were most similar to each other and were most closely related to Ty3 polymerases present in the same clade of planarians that Burro is found in. This suggests that the polymerase that drives Burro elements did not come from outside the planarian genome but rather was already present in the genome.

(E) Phylogenetic tree of the planarian type I BIR-domain proteins (IAP proteins). The BIR-domain protein that is the main topic of this study is only present in Burro1. Based on phylogenetic analysis it is clearly derived from one of the *iap* genes in the planarian genome called *iap-2*. Numbers above the branches represent Bayesian posterior probabilities (> 90). Numbers below branches are ML bootstrap support percentages (> 50). (D,E).

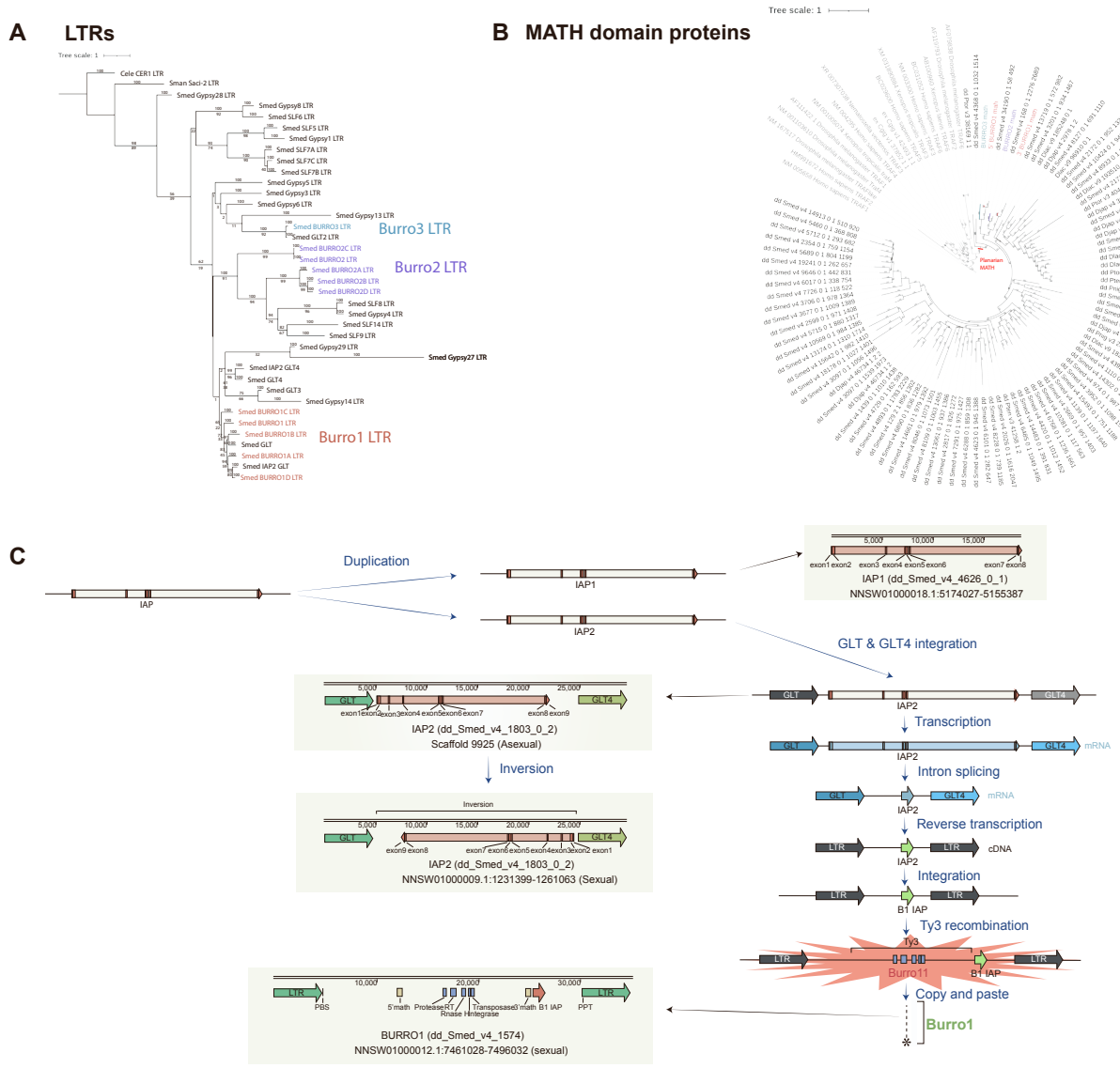

Figure S2. Life history of Burro1 continued. Related to Figure 1.

(A) Phylogenetic tree of LTRs of the Burro elements relative to the LTRs of other planarian Ty3 elements. The LTRs are quite distinct between Burro1, Burro2, and Burro3, suggesting that the core retrotransposon genes acquired different LTRs. This could have happened for example by insertion into different locations. All Burro LTRs have resemblance to planarian Ty3 sequences: the LTRs of Burro2 and Burro3 resemble the LTRs of other Ty3s , whereas the LTR of Burro1 shows strong similarity to a full Ty3 element of the GLT subfamily, inparticular one that is found adjacent to *iap-2*.

(B) Phylogenetic tree of the MATH domain proteins of the Burro elements relative to other metazoan MATH domain proteins. The additional Open Reading Frames (ORFs) are unique to the Burro elements. They include a 5' MATH domain protein that is present in Burro1 and Burro3 and a 3' MATH domain protein is present in Burro1 and Burro2. There are many MATH domain proteins in the planarian genome and therefore it is difficult to determine the exact origin of these elements. The four MATH domain proteins in the Burro elements are related to each other, and are clearly related to other planarian MATH domain proteins, but we were unable to determine an exact founder sequence.

Numbers below branches are ML bootstrap support percentages (> 50) (A,B).

(C) Schematic representing the hypothesized series of events leading to the birth of the Burro1 element (expanded from Figure 1H). Burro1 is easily distinguished from the other Burro elements by the presence of B-IAP and by the LTR elements that are related to GLT. Remarkably, *iap-2* is flanked in the genome by two GLT elements, and one of them is highly similar to the Burro1 LTR. This suggests that the *iap-2* sequence and the flanking LTR may have become part of Burro1 together. The *iap-2* sequence in the genome has multiple introns, whereas the sequence in Burro1 is a cDNA copy. Remarkably we also found in the genome another copy of the *iap-2* cDNA flanked by GLT elements. While it is not possible to know with certainty how the GLT sequence and the *iap* cDNA became part of Burro1, we favor the idea that a transcript initiated from the GLT element could have been spliced and reverse transcribed and inserted back in the genome, after which the core Ty3 element jumped into such a location. Alternatively, transcripts from the GLT-*iap-2* locus may have been processed together with transcripts of the core Burro genes leading to a merged reverse transcribed product that then was inserted into the genome.

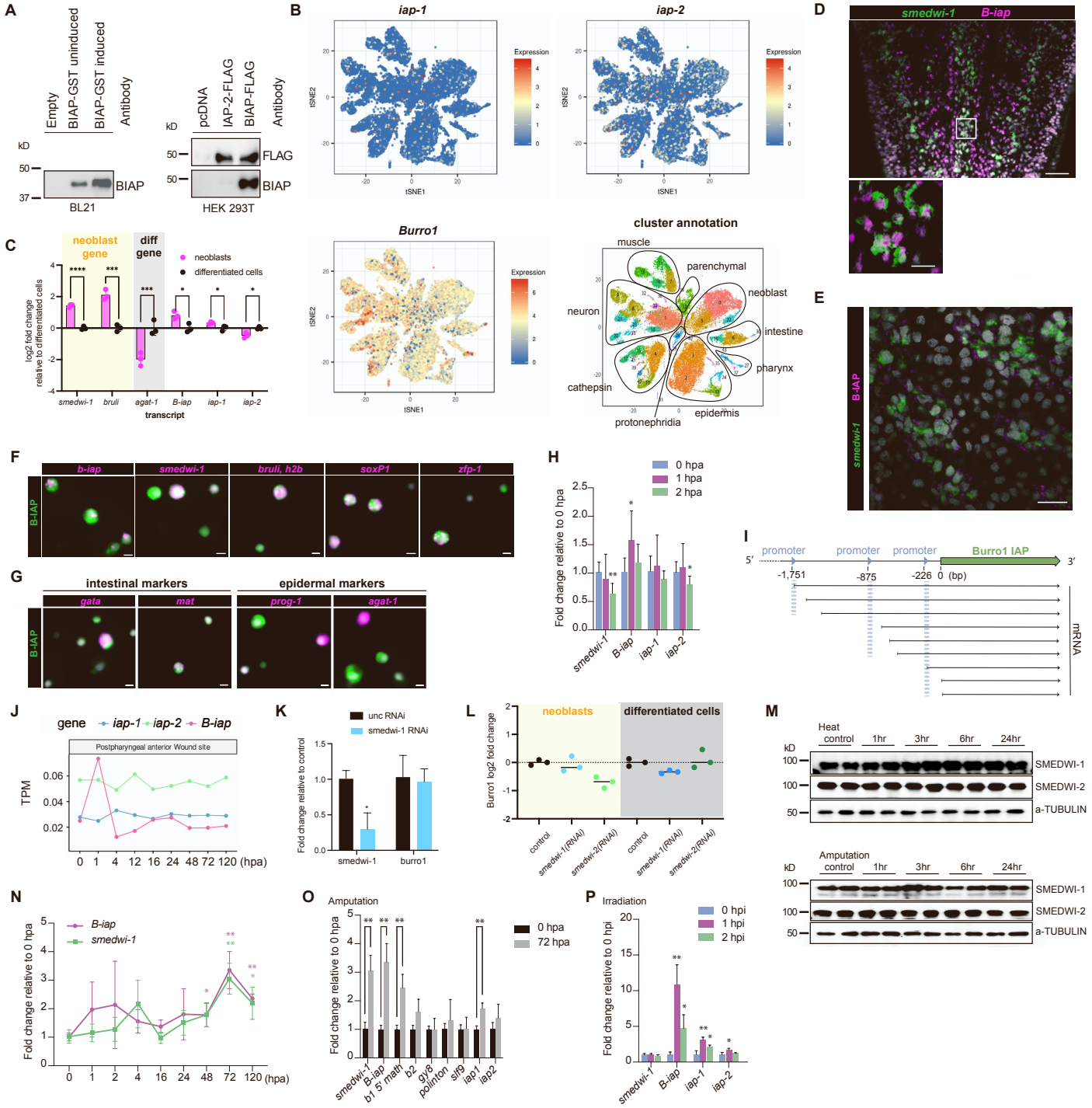

Figure S3. Regulation of *Burro-iap (B-iap)*. Related to Figures 2,3.

(A) Western blot showing the specific detection of B-IAP constructs expressed in bacterial (BL21), or mammalian (HEK293T) cells by the B-IAP antibody.

(B) UMAP representation as generated on https://digiworm.wi.mit.edu showing the expression of planarian *iap* genes in a public single cell RNAseq data set [S1]. Bottom right: Interpretation of the various cell types on the UMAP plot.

(C) qPCR on isolated neoblasts and differentiated cells shows enrichment of neoblast transcripts *smedwi-1* and *bruli* (yellow shading) in the neoblasts and depletion of epidermal transcript *agat-1* (grey shading). The transcripts of *B-iap and iap-1* are mildly enriched in the neoblasts, whereas *iap-2* is mildly depleted. Significance: *p ≤ 0.05, **p ≤ 0.01, ***p ≤ 0.001, ****p ≤ 0.0001 by Student's t-test; n=3 samples of sorted cells, from 12 dissociated animals each.

(D) Fluorescent in situ hybridization (FISH) on whole mount animals showing *B-iap* (magenta) together with the neoblast marker *smedwi-1*(green). Bottom panel shows zoomed in section. *B-iap* is expressed in the neoblasts. Scale bars: 50 μm (top) and 10 mm (bottom).

(E) (expanded from Figure 2H) Immunostaining of intact planarians for the B-IAP protein (magenta) with FISH for the neoblast marker *smedwi-1* (green) shows granules of B-IAP protein associated with the neoblasts. Scale bar: 20 μm.

(F) Immunofluorescence on isolated cells shows co-expression of B-IAP (green) with FISH for the stem cell markers *smedwi-1, bruli, h2b, soxP1*, and *zfp-1* (magenta). Scale bar: 5μm.
(G) Immunofluorescence on isolated cells shows co-expression of B-IAP (green) with FISH for the intestinal markers *gata456* and *mat* (magenta), but not with epidermal precursor markers *prog-1* and *agat-1* (magenta). Scale bar: 5μm.
(H) qPCR on tissue fragments in the early hours upon head amputation shows an increase of *B-iap* transcript at 1 hour after amputation. The size of the effect can vary between experiments, but the direction is consistent. Significance: *p ≤ 0.05, **p ≤ 0.01. Data shown as mean ± SD: n=3 samples of individual animals.
(I) Location of putative internal promoters in Burro1, and the identified 5' ends of B-IAP transcripts. To determine where transcription was initiated, we performed 5' RACE. We found presence of long transcripts that initiated at the start of Burro1, but also found a significant number of transcripts that originated from a region just upstream of the B-IAP ORF. TSS prediction [S2] showed several sites with high likelihood of TSS activity at the end of the polyprotein, and additionally predicted two sites just upstream of *B-iap*, matching the sites identified by the 5' RACE. This indicates that *B-iap* is likely in part transcribed from internal Burro1 promoters and could be activated independently of the transcription of the core polyprotein. However, in experiments where we measured upregulation of *B-iap* transcript in response to stress we never detected a difference in RNA level between the *B-iap* part of Burro1 and the polymerase part.
Ty3 elements are often transcribed from a TSS in their 5' LTR [S3]. In some cases, transcription factors have been identified to activate this transcription. For example, in yeast, the transcription factor Ste12, which is activated in response to mating pheromone, enhances transcription of Ty3 [S4, S5]. Planarians encode many transcription factors (TFs), and the stress-induced upregulation of Burro1 suggests that transcription must be regulated. However, no binding motifs of planarian TFs have been experimentally determined, complicating the prediction of TFs involved in this process. Additionally, we recently reported that transcription of planarian stem cell genes does not appear to depend on specific TFs. Rather, the encoded accessibility of the promoter regions of stem cell genes makes them default targets for transcription [S6]. We hypothesize that something similar may be at play at the transposon loci, where stress could make the LTRs more accessible resulting in increased transcription independent of specific transcription factor-based regulation. This could explain the rapid response and the wide range of stresses that induce Burro1 transcripts.
(J) Analysis of public sequencing data from wound response timecourses [S7] confirms the presence of an early and a delayed increase in *B-iap* levels.
(K) qPCR after RNAi-mediated knockdown of *smedwi-1* shows no significant changes in transcript levels of Burro1, indicating that detected changes in *B-iap* levels are not caused by changes in *smedwi-1* levels upon stress. Significance: *p ≤ 0.05. Data shown as mean ± SD: n=3 samples of 2 animals each.
Transposon transcripts are commonly silenced by RNA-based cellular defense mechanisms such as siRNAs and piRNAs. piRNAs and their mediators the PIWI proteins, are prominently present in the planarian stem cells and play important roles in planarian biology. *S. mediterranea* encodes 3 PIWI proteins, of which 2 are cytoplasmic (SMEDWI-1, and SMEDWI-3) and limited to the stem cells, whereas the third (SMEDWI-2) is nuclear and remains present in differentiated cells as well [S8]. piRNAs targeting Burro1 are found among the piRNAs bound to both SMEDWI-1 and SMEDWI-2, indicating that Burro1 is subject of this silencing mechanism. SMEDWI-1 and SMEDWI-2 redundantly mediate silencing in the stem cells [S9]. We previously reported that loss of SMEDWI-2 leads to upregulation of Burro1 specifically in the intestinal cells, even though the piRNAs targeting Burro1 are present in all cell types [S8]. This corresponds with our finding in this study that the B-IAP protein can be detected in cells that express intestinal markers, but not in cells that express epidermal markers (see Figure S3G). We previously reported that some activated Burro1 copies were located in proximity to intestinal genes, and we hypothesize that the increased accessibility of these regions in intestinal cells permits the transcription of Burro1.
(L) qPCR on isolated neoblasts (reproduced from [S9]) and isolated differentiated cells after RNAi-mediated knockdown of *smedwi-1* or *smedwi-2* shows no significant changes in transcript levels of Burro1, indicating that detected changes in *B-iap* levels are not caused by changes in *smedwi-1* levels upon stress. Significance: not significant by Student's t-test; n=3 samples of sorted cells, from 12 dissociated animals each.
(M) Western blots showing protein levels of SMEDWI-1 and SMEDWI-2 during the first 24 hours after amputation or heat stress. No decrease in protein levels was detected.
(N) qPCR time course of *B-iap* levels after amputation. An immediate increase in *B-iap* is detected at 1-2 hours after amputation (hpa). Later, around 3 days after amputation an increase in *B-iap* is detected commensurate with the increase in the neoblast marker *smedwi-1*. Significance: *p ≤ 0.05, **p ≤ 0.01 by Student's t-test. Data shown as mean ± SD: n=3 samples of individual isolated wound sites each.
(O) qPCR on tissue fragments at 72h after amputation shows an increase in *B-iap* transcript commensurate with the increase in *smedwi-1* transcript. Significance: *p ≤ 0.05, **p ≤ 0.01 by Student's t-test. Data shown as mean ± SD: n=5 samples of 3 animals each.
(P) qPCR at early timepoints after irradiation (2500Rads) in combination with drought shows an increase in *B-iap* transcript at 1 hour and 2 hours after treatment. Significance: *p ≤ 0.05, **p ≤ 0.01 by Student's t-test. Data shown as mean ± SD: n=5 samples of 3 animals each.

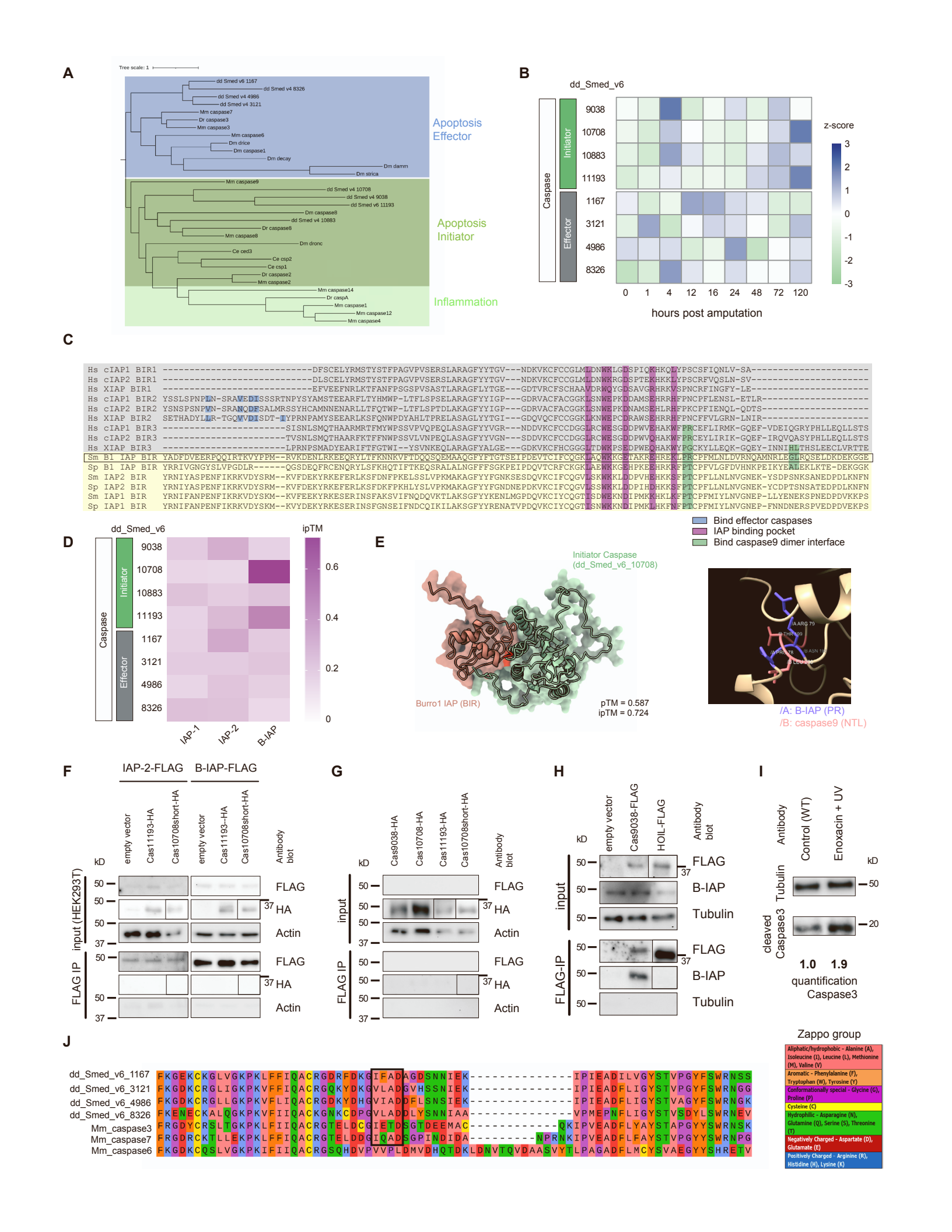
A
Tree scale: 1
dd Smed v6 1167
dd Smed v4 8326
dd Smed v4 4986
dd Smed v4 3121
Mm caspase7
Dr caspase3
Mm caspase3
Mm caspase6
Dm drice
Dm caspase1
Dm decay
Dm damm
Dm strica
Mm caspase9
dd Smed v4 10708
dd Smed v6 9038
dd Smed v6 11193
Dm caspase8
dd Smed v4 10883
Dr caspase8
Mm caspase8
Dm dronc
Ce ced3
Ce csp2
Ce csp1
Dr caspase2
Mm caspase2
Mm caspase14
Dr caspA
Mm caspase1
Mm caspase12
Mm caspase4
Apoptosis Effector
Apoptosis Initiator
Inflammation
B
dd_Smed_v6
Caspase
Initiator
Effector
9038
10708
10883
11193
1167
3121
4986
8326
0 1 4 12 16 24 48 72 120
hours post amputation
z-score
3 2 1 0 -1 -2 -3
C
Hs cIAP1 BIR1
Hs cIAP2 BIR1
Hs XIAP BIR1
Hs cIAP1 BIR2
Hs cIAP2 BIR2
Hs XIAP BIR2
Hs cIAP1 BIR3
Hs cIAP2 BIR3
Hs XIAP BIR3
Sm B1 IAP BIR
Sp B1 IAP BIR
Sm IAP2 BIR
Sp IAP2 BIR
Sp IAP1 BIR
Sm IAP1 BIR
Sp IAP1 BIR
D
dd_Smed_v6
Caspase
Initiator
Effector
9038
10708
10883
11193
1167
3121
4986
8326
IAP-1
IAP-2
B-IAP
ipTM
0.6
0.4
0.2
0
E
Initiator Caspase
(dd_Smed_v6_10708)
Burro1 IAP (BIR)
pTM = 0.587
ipTM = 0.724
Bind effector caspases
IAP binding pocket
Bind caspase9 dimer interface
/A: B-IAP (PR)
/B: caspase9 (NTL)
F
IAP-2-FLAG
B-IAP-FLAG
empty vector
Cas11193-HA
Cas10708short-HA
Antibody blot
kD
input (HEK293T)
FLAG IP
FLAG
HA
Actin
G
Cas9038-HA
Cas10708-HA
Cas11193-HA
Cas10708short-HA
input
FLAG IP
H
empty vector
Cas9038-FLAG
HOIL-FLAG
B-IAP
Tubulin
FLAG-IP
I
Antibody
Control (WT)
Enoxacin + UV
Tubulin
cleaved Caspase3
1.0 1.9
quantification Caspase3
J
dd_Smed_v6_1167
dd_Smed_v6_3121
dd_Smed_v6_4986
dd_Smed_v6_8326
Mm_caspase3
Mm_caspase7
Mm_caspase6
Zappo group
Aliphatic/hydrophobic - Alanine (A), Isoleucine (I), Leucine (L), Methionine (M), Valine (V)
Aromatic - Phenylalanine (F), Tryptophan (W), Tyrosine (Y)
Conformationally special - Glycine (G), Proline (P)
Cysteine (C)
Hydrophilic - Asparagine (N), Glutamine (Q), Serine (S), Threonine (T)
Negatively Charged - Aspartate (D), Glutamate (E)
Positively Charged - Arginine (R), Histidine (H), Lysine (K)

Figure S4. Burro-IAP (B-IAP) is a functional anti-apoptotic protein. Rrelated to Figure 4.
(A) Phylogenetic tree of *S. mediterranea* caspases (dd IDs [S10]) together with caspases from mouse (Mm), zebrafish (Dr), *Drosophila* (Dm), and *C. elegans* (Ce). Caspases are cysteine proteases and typically cleave after a 4-amino acid motif that ends in an aspartate [S11]. Caspases exist in two major types: effector caspases, which cleave cellular proteins during apoptosis, initiator caspases, which cleave the effector caspases to activate them. Additionally, vertebrates encode caspases that are involved in inflammation. Effector caspases typically target DEVD motifs, while initiator caspases have more variation in their target motif.
The *S. mediterranea* genome encodes 8 caspases, of which 4 cluster with initiator caspases from other model systems, and the other 4 cluster with effector caspases. Nevertheless, the planarian caspases cannot be assigned direct mammalian homologs and within each type they resemble each other more than they resemble the mammalian caspases of the type. For this reason we could not assign animo acid motifs known to be targeted by specific mammalian initiator caspases to the planarian ones.
(B) Analysis of public sequencing data from wound response timecourses [S7]. All four initiator caspases were upregulated around 4 hours after amputation.
(C) Alignment of relevant sections of the BIR domains from planarian (yellow shading) *S. mediterranea* (Sm) and *S. polychroa* (Sp) IAP proteins with human (Hs - grey shading) IAP proteins, indicating the positions of conserved residues for Caspase-3 and Caspase-9 interaction. B-IAP retains the residues required for interaction with Caspase-9, but not those required for the interaction with Caspase-3.
(D) (expanded from Figure 4A) Heatmap showing the likelihood of interaction between the three planarian IAP proteins and the various planarian caspases (dd IDs [S10]). ipTM: confidence score for the interaction. Only the interaction between B-IAP and the initiator caspase has significant support.
(E) Model of the predicted interaction between the BIR domain of B-IAP and the planarian initiator Caspase. pTM: confidence score for the structure; ipTM: confidence score for the interaction. The location of the conserved amino acids of the BIR domain that interact with the caspase are indicated by a red box and enlarged in the ribbon model on the right.
(F) (ad Figure 4B) Western blots showing coIPs of additional HA-tagged Caspases with FLAG-tagged IAP protein expressed in HEK293T cells. No interactions were identified for caspase_11193 or for caspase_10708 without its N-terminal region. Blot regions shown are selected to match the expected size of the protein product.
(G) (ad Figure 4B, negative control) Western blots showing no binding of HA-tagged Caspases to FLAG-binding beads exposed to HEK293T cell lysate.
(H) (expanded from Figure 4C, negative control) Western blots showing that B-IAP protein is pulled down by the FLAG-tagged Caspase_9038, but not by an unrelated FLAG-tagged protein (HOIL) or by FLAG-binding beads exposed to HEK293T cell lysate.
(I) Western blots showing that treatment with enoxacin and UV results in an increase of activated caspase3. Quantification relative to Tubulin.
(J) Alignment of the relevant regions of the effector caspases from *S. mediterranea* (dd IDs [S10]) and from mouse (Mm). A box marks the location of the cleavage site. To identify the target motif of the planarian initiator caspases, we aligned the planarian effector caspases with mouse effector caspases and identified the activating intrachain cleavage site present in the mouse effector caspases. Inspection of the corresponding position in the planarian effector caspases revealed a clear VLAD motif. As this cleavage is performed by the initiator caspases, we deduced that the planarian initiator caspase cleavage preference must be a VLAD motif.

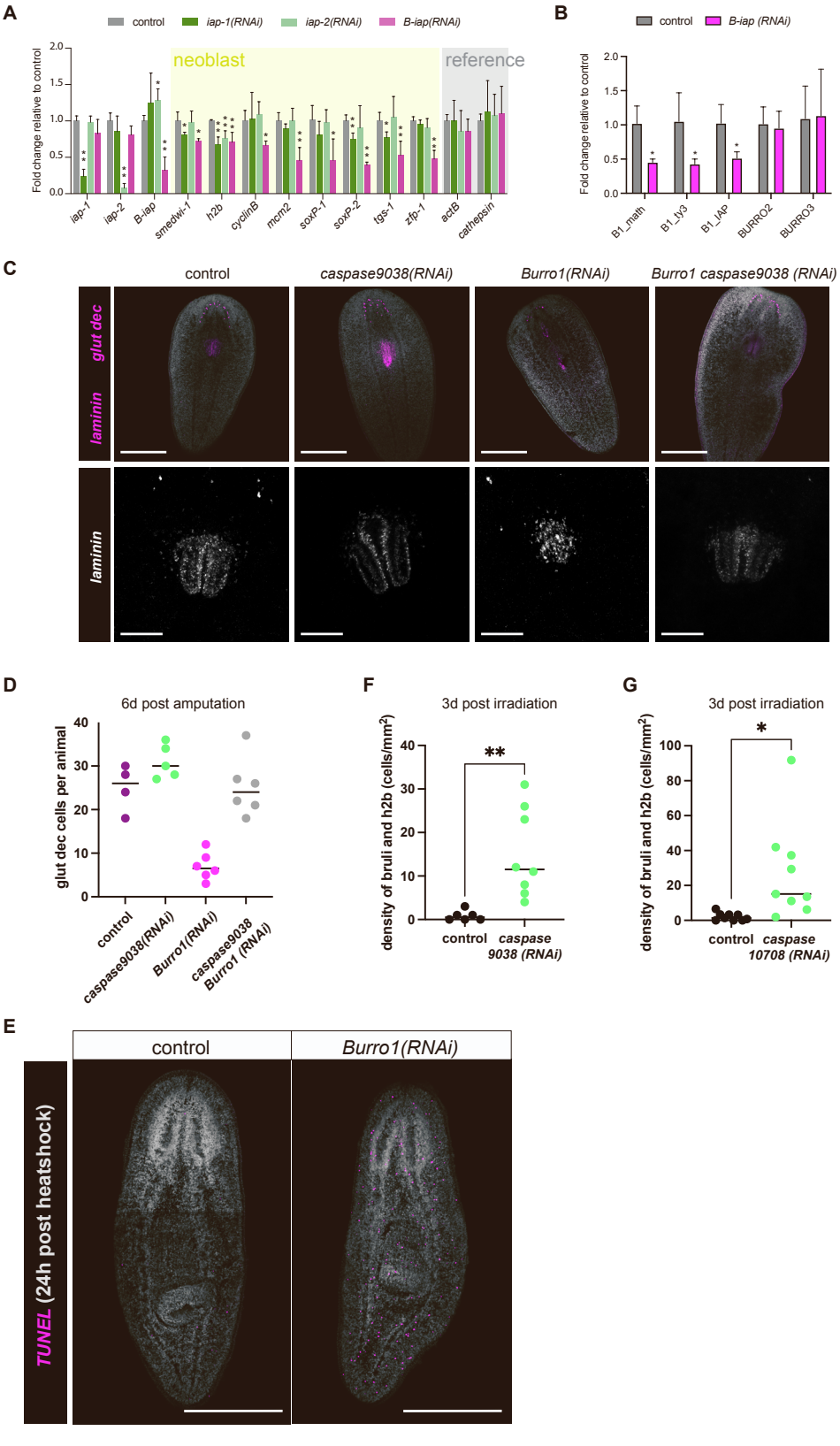
A
control
iap-1(RNAi)
iap-2(RNAi)
B-iap(RNAi)
Fold change relative to control
neoblast
reference
iap-1
iap-2
B-iap
smedwi-1
h2b
cyclinB
mcm2
soxP-1
soxP-2
tgs-1
zfp-1
actB
cathepsin
B
control
B-iap (RNAi)
Fold change relative to control
B1_math
B1_ly3
B1_IAP
BURRO2
BURRO3
C
control
caspase9038(RNAi)
Burro1(RNAi)
Burro1 caspase9038 (RNAi)
glut dec
laminin
laminin
D
6d post amputation
glut dec cells per animal
control
caspase9038(RNAi)
Burro1(RNAi)
caspase9038 Burro1 (RNAi)
F
3d post irradiation
density of bruli and h2b (cells/mm2)
control
caspase 9038 (RNAi)
G
3d post irradiation
density of bruli and h2b (cells/mm2)
control
caspase 10708 (RNAi)
E
control
Burro1(RNAi)
TUNEL (24h post heatshock)

Figure S5. Burro1 supports regeneration in *S. mediterranea*. Related to Figure 5.
(A) qPCR quantification of *iap* transcript levels upon RNAi-mediated knockdown of each of the *iap* genes. Neoblast genes are marked by yellow shading; housekeeping genes by grey shading. Significance: *p ≤ 0.05, **p ≤ 0.01 by Student's t-test. Data shown as mean ± SD; n=3 individual animals.
(B) qPCR quantification of Burro1 core sequence , the 5' Math region, and *B-iap* transcript levels, as well as levels of Burro2 and Burro3 upon RNAi-mediated knockdown of the *B-iap* sequence. Significance: *p ≤ 0.05 by Student's t-test. Data shown as mean ± SD; n=3 samples of 2 animals each.
(C) Representative FISH images of regenerating tail pieces of control animals *caspase9(RNAi)* animals, *Burro1(RNAi)* animals, and *caspase9 Burro1 (double RNAi)* animals at 6 days after amputation. Shown are neuronal marker glutamate decarboxylase and pharynx marker laminin (top) or a zoomed in view of laminin (bottom). Scale bars: 300 μm (top) and 100 μm (bottom). n=4 control animals; 5 *caspase9(RNAi)* animals; 6 *Burro1(RNAi)* animals, and *caspase9 Burro1 (double RNAi)* animals each.
(D) Quantification of the neuronal marker shown in C.
(E) (expanded from Figure 5K to show DAPI signal) Representative image (tile scan) of FISH staining for neoblast markers (*bruli* and *h2b*) on control and *Burro1(RNAi)* animals 3 days after 1250Rads of irradiation, showing reduced neoblast survival in the *Burro1(RNAi)* animals. Scale bars: 300 μm.
(F) Quantification of the density of neoblasts at 3 days after irradiation at 2000Rads in control animals or *caspase_9038(RNAi)* animals shows increased neoblast survival in the *caspase(RNAi)* animals. Significance: **p ≤ 0.01, by Student's t-test. n=6 control animals; 8 *caspase9038(RNAi)* animals.
(G) Quantification of the density of neoblasts at 3 days after irradiation at 3000Rads in control animals or *caspase_10708(RNAi)* animals shows increased neoblast survival in the *caspase(RNAi)* animals. Significance: *p ≤ 0.05 by Student's t-test. n=9 control animals; 9 *caspase10708(RNAi)* animals.

RNAi& DNA standards for genomic qpcr quantification (plasmid)	BURR1 IAP	A	GGACCAGATTCGATATGGACGA
		B	AAGCTGGAGCTCCACCGCGGACTACGACGGAACAAGACGG
		C	GGGCGAATTGGGTACCGGGCCTCTTCTCGCTCTTGGTACG
	Gypsy8	B	AAGCTGGAGCTCCACCGCGGAGACCGTATAAAATCCCACAAAGC
		C	GGGCGAATTGGGTACCGGGACCCCGTCAAACCTAAGAATCC
		D	TCCTTTCTTCTCTAGGACAGTCA
	BURRO2	A	AGCCGTTATTGCTTTGTCTCT
		B	AAGCTGGAGCTCCACCGCGGTGCTTTGTCTCTTGCTTTGATT
		C	GGGCGAATTGGGTACCGGGCAGCAAGCAGAGACATCCCA
	B1 5' MATH	A	GCGAGAACGAACCCCGATAT
		B	AAGCTGGAGCTCCACCGCGGTGGGAAGACGGACAAACCAT
		C	GGGCGAATTGGGTACCGGGGTTTGGGTTGTTCGTCTGCC
	SLF9	A	GTTGAGGAAAGGAGCACCGA
		B	AAGCTGGAGCTCCACCGCGGACTACCGAGCATAGATGAGATGA
		C	GGGCGAATTGGGTACCGGGCGGTTTCACGTCCTCTTCCA
nanopore & 5' race reverse primer	B1_reverse	1	ACTTGCCTGTCGCTCTATCTTCCCTCTTGTTCTAAAGCTTCCTCTTGC
		2	ACTTGCCTGTCGCTCTATCTTCCTGGATCTTTGGTTGTGGTTCGTAC
		3	ACTTGCCTGTCGCTCTATCTTCGGGTGTACGAGTATTGGTGCTGATA
		4	ACTTGCCTGTCGCTCTATCTTCATCAGCGAAACGGAATCCTTTGATC
		5	ACTTGCCTGTCGCTCTATCTTCCTGGGTTGATCTTGAGGGGTGATTG
pcdna	B-IAP	F	AAAAAGCTTGCCACCATGGCAAGCGGAATCAGCGAAG
		R	AAAGGATCCTCACTTATCGTCGTCATCCTTGTAATCCTGATCAGCGAAACGGAATC
qPCR	b1 5' math	F	CCAAACGGAGATGGGGTAGGA
		R	CCCATTTTCCGGGTTTAGCGA
	b1 iap	F	GCAATCAAGCGATATCAAGAGAAACC
		R	CTGCCAACATGTCACACATTGAT
	burro2	F	ACAGAGAGATCAGACGATTGGAGT
		R	TTTCTCTTCTCGTTGCATTTTCTGTT
	slf9	F	ACAATGGCGGATGGGAAGAGT
		R	TGCCACCAATGAATTCGTCGT
	gy8	F	TGGACGACGAAGAGTGCTGT
		R	TCGTTGTGCCGGTAGATGGG
	iap2	F	TCAAGATTCGCTAATAAAGTCGAGC
		R	GCATTGAATCATAATCCTTGCCGG
	iap1	F	TCGCAAAGAGTCTGAACGTATAAATTCA
		R	CTTGATCGGGTCCCATTAAATTCTC
	smedwi-1	F	AAGAAGATTCGCAATTATTGAACC
		R	TCTTCCATCTTTCCCTATTTTGTC
	h2b	F	TAACCAGCAGAGAGATTCAAACTG
		R	GTTCCTTCACTAACTGCGTGTTTA
	cyclinB	F	AGCAGCCAGTGGACTCGTTT
		R	TAATTGCCCGAAATTTTGAAAAAGTTGC
	mcm2	F	TAACATCAATTTCATCTCCAGGCTTGC
		R	GAGAGTCCCGGTACTGTTCCG
	soxP-1	F	ACCCATTACCTCCTGAATGGCT
		R	TGGTTGGACGTCGCCTTCTT
	soxP-2	F	CTTCCCAAGAAGTTTGCTTATTTCTGA
		R	GGCCATTGAATAGTTTCATGATATTTTCCA
	tgs1	F	GCCAACACTGAAAAATCAAACGTTGA
		R	CGCTGCTAGCTTTCGCTTCT
	zfp-1	F	CCCGTGCCTGAACAATTTGACA
		R	CCTCAGCGCATGCCTCTGTA
	actB	F	AGCCCCTGAAGAACATCCAGT
		R	GCGGGCGCATTGAATGTTTC
	H1	F	TCAAGCCAGGATCGCACAGG
		R	CGACGCAAAAACGGACCGTA
	H3	F	AGAGGGCCGTAACGCATTCT
		R	CGCTAAACGTGTTACAATTATGCCG
	gapdh	F	TCTTCCCCAACCAATTTTCTGTTCTG
		R	CCGAATATTTTATTTGGCTCTTCCTCCA
	ubiquilin	F	AAATTCGCCTGCCTGTTGGG
		R	CCGGTGGCATTAATCCATCTGT
B1 integration in piwi4 intron	Primer	1F	TATTTTGTCACGCTTTTAGCCTATC
	Primer	2R	CCGGACCTTAAGTCCATCTTT
	Primer	3F	CATAATTCTCTGTTGTTTCTTAACTTG
	Primer	4R	GGGTTGTATCCATAAAAAGTTCAGA
pGEX	B-IAP GST	F	GATGGATCCATGGCAAGCGGAATCAGCG
		R	AGCGGCCGCTATTGGTTTCTGACGTCTAA
pcdna	BIAP_3XFLAG	F	AAAAAGCTTGCCACCATGGCAAGCGGAATCAGCGAAG
		R	AAAGGATCCTCACTTGTCGTCGTCGTCCTTGTAGTCGATGTCGTGGTCCTTGTAGTCACCGTCGTGGTCCTTGTAGTCCTGATCAGCGAAACGGAATC
	IAP2_3XFLAG	F	AAAAAGCTTGCCACCATGTCTACCATAAATCTTCAA
		R	AAAGGATCCTCACTTGTCGTCGTCGTCCTTGTAGTCGATGTCGTGGTCCTTGTAGTCACCGTCGTGGTCCTTGTAGTCAGAAGTTGTATTCCCATCAA
	Cas9038_3XFLAG	F	TTGGTACCGCCACCATGAATTATTATAAATTTTTGC
		R	AAAGGATCCTCACTTGTCGTCGTCGTCCTTGTAGTCGATGTCGTGGTCCTTGTAGTCACCGTCGTGGTCCTTGTAGTCCAATATATCAATAAAATCGA
	Cas10708short_3xHA	F	AAAAAGCTTGCCACCATGTGCAGAATACGAAATGGCTT
		R	AAAAGAATTCTCAAGCGTAATCTGGAACATCGTATGGGTAAGCAAATGAACAATCCTCTCG
		2R	AAAGGATCCTCAAGCGTAATCGGGCACATCATATGGGTAGGCGTAGTCTGGGACATCGTAAGGGTAAGCGTAATCTGGAACATCGTATGGGTA
	Cas10708_3xHA	F	AAAAAGCTTGCCACCATGGATTTCTTTATGATATATTTG
		R	AAAAGAATTCTCAAGCGTAATCTGGAACATCGTATGGGTAAGCAAATGAACAATCCTCTCG
		2R	AAAGGATCCTCAAGCGTAATCGGGCACATCATATGGGTAGGCGTAGTCTGGGACATCGTAAGGGTAAGCGTAATCTGGAACATCGTATGGGTA
	Cas11193_3xHA	F	AAAAAGCTTGCCACCATGAGTAAATACGACATTGA
		R	AAAAGAATTCTCAAGCGTAATCTGGAACATCGTATGGGTAAATAAAATCACCGAAATCAC
		2R	AAAGGATCCTCAAGCGTAATCGGGCACATCATATGGGTAGGCGTAGTCTGGGACATCGTAAGGGTAAGCGTAATCTGGAACATCGTATGGGTA

Table S1. Primer sequences used in this study. Related to STAR Methods.

Table S2. Sequences used in the phylogenetic analysis (related to STAR Methods)
Provided as a separate excel file.

Supplemental References

S1. Fincher, C.T., Wurtzel, O., de Hoog, T., Kravarik, K.M., and Reddien, P.W. (2018). Cell type transcriptome atlas for the planarian Schmidtea mediterranea. Science *360*. 10.1126/science.aaq1736.

S2. Wurtzel, O., Cote, L.E., Poirier, A., Satija, R., Regev, A., and Reddien, P.W. (2015). A Generic and Cell-Type-Specific Wound Response Precedes Regeneration in Planarians. Dev Cell *35*, 632-645. 10.1016/j.devcel.2015.11.004.

S3. Li, D., Taylor, D.H., and van Wolfswinkel, J.C. (2021). PIWI-mediated control of tissue-specific transposons is essential for somatic cell differentiation. Cell Rep *37*, 109776. 10.1016/j.celrep.2021.109776.

S4. Allikka Parambil, S., Li, D., Zelko, M., Poulet, A., and van Wolfswinkel, J.C. (2024). piRNA generation is associated with the pioneer round of translation in stem cells. Nucleic Acids Res *52*, 2590-2608. 10.1093/nar/gkad1212.

S5. Grohme, M.A., Schloissnig, S., Rozanski, A., Pippel, M., Young, G.R., Winkler, S., Brandl, H., Henry, I., Dahl, A., Powell, S., et al. (2018). The genome of Schmidtea mediterranea and the evolution of core cellular mechanisms. Nature *554*, 56-61. 10.1038/nature25473.

S6. Julien, O., and Wells, J.A. (2017). Caspases and their substrates. Cell Death Differ *24*, 1380-1389. 10.1038/cdd.2017.44.

S7. Reese, M.G. (2001). Application of a time-delay neural network to promoter annotation in the Drosophila melanogaster genome. Comput Chem *26*, 51-56. 10.1016/s0097-8485(01)00099-7.

S8. Boeke, J.D., and Corces, V.G. (1989). Transcription and reverse transcription of retrotransposons. Annu Rev Microbiol *43*, 403-434. 10.1146/annurev.mi.43.100189.002155.

S9. Van Arsdell, S.W., Stetler, G.L., and Thorner, J. (1987). The yeast repeated element sigma contains a hormone-inducible promoter. Mol Cell Biol *7*, 749-759. 10.1128/mcb.7.2.749-759.1987.

S10. Bilanchone, V.W., Claypool, J.A., Kinsey, P.T., and Sandmeyer, S.B. (1993). Positive and negative regulatory elements control expression of the yeast retrotransposon Ty3. Genetics *134*, 685-700. 10.1093/genetics/134.3.685.

S11. Poulet, A., Kratkiewicz, A.J., Li, D., and van Wolfswinkel, J.C. (2023). Chromatin analysis of adult pluripotent stem cells reveals a unique stemness maintenance strategy. Sci Adv *9*, eadh4887. 10.1126/sciadv.adh4887.